Structural, Conformational, and Spectroscopic Studies of Primary Amine Complexes of Iron(II) Porphyrins

Orde Q. Munro,*,† P. Sizwe Madlala,† Richard A. F. Warby,† Takele B. Seda,‡ and Giovanni Hearne‡

School of Chemical and Physical Sciences, University of Natal, Private Bag X01, Scottsville, Pietermaritzburg 3209, South Africa, and Department of Physics, University of the Witwatersrand, P.O. Wits 2050, Johannesburg, South Africa

Received February 25, 1999

Three novel bis(primary amine)iron(II) porphyrins [Fe(TPP)(RNH_2)$_2$], where RNH_2 = 1-butylamine, benzylamine, and phenethylamine, have been synthesized and characterized by X-ray crystallography and IR, electronic, and Mössbauer spectroscopy. The compounds provide unprecedented structural data for the coordination of primary amines by iron(II) porphyrins. The Fe−N_{ax} distances of [Fe(TPP)(1-$BuNH_2$)$_2$], [Fe(TPP)($BzNH_2$)$_2$], and [Fe(TPP)($PhCH_2CH_2NH_2$)$_2$] are 2.039(3), 2.043(3), and 2.028(2) Å, respectively. The Fe−N_p distances of the three complexes average 1.990(2) Å. The zero-field Mössbauer spectra (5−300 K) show comparable isomer shifts (0.393(1)−0.493(1) mm/s) and quadrupole splittings (1.144(6)−1.204(3) mm/s) that are consistent with an S = 0 iron(II) assignment in each case. The bis(primary amine) complexes are structurally and spectroscopically similar to [Fe(TPP)(Py)$_2$] derivatives, where Py = an unsubstituted pyridine. Molecular mechanics (MM) calculations with a force field parametrized for primary and secondary amine complexes of iron(II) porphyrins show that stable conformations arise when the α-CH_2 and NH_2 protons of the coordinated ligands are staggered relative to the Fe−N_p bonds of the porphyrin core. The lowest energy conformations of the three [Fe(TPP)(RNH_2)$_2$] complexes therefore have the ligand α-carbons positioned directly over the Fe−N_p bonds of the porphyrin core. The X-ray structure of [Fe(TPP)($PhCH_2CH_2NH_2$)$_2$] lies close to the global minimum (ϕ_1, ϕ_2 = 0, 180°) on the potential surface, while [Fe(TPP)($BzNH_2$)$_2$] and [Fe(TPP)(1-$BuNH_2$)$_2$] show deviations that may be attributed to packing interactions in the solid and intrinsically low barriers to axial ligand rotation (<0.5 kcal/mol). Three types of minimum energy conformation are accessible for [Fe(TPP)(Pip)$_2$]. The lowest energy conformation has an S_4-ruffled porphyrin core. The conformation which matches the X-ray structure (Radonovich, L. J.; Bloom, A.; Hoard, J. L. *J. Am. Chem. Soc.* **1972**, *94*, 2073−2078) is a local minimum (1.6 kcal/mol higher in energy than the global minimum) with exact inversion symmetry. Higher in vacuo strain energy barriers (∼2.2 kcal/mol) separate the potential minima of [Fe(TPP)(Pip)$_2$], consistent with the increased bulk of the secondary amine axial ligands.

Introduction

Six-coordinate imidazole and pyridine complexes of Fe(II) porphyrins have been amply characterized by crystallographic,[1−5] spectroscopic,[6−8] and computational methods[8,9] over the last two decades. These efforts largely reflect an attempt to understand the functional role of the axial ligands in the bis(histidine) cytochromes b[10−16] and c[17−19] which cycle between the Fe(II) and Fe(III) oxidation states in vivo. In contrast, the coordination of alkylamine ligands by both Fe(II) and Fe(III) porphyrins remains relatively unexplored. However, the recent 1.96-Å resolution X-ray structure of turnip cytochrome *f* has shown

* To whom correspondence should be addressed. Electronic mail: MunroO@chem.unp.ac.za.

† University of Natal, Pietermaritzburg.

‡ University of the Witwatersrand.

(1) Safo, M. K.; Scheidt, W. R.; Gupta, G. P. *Inorg. Chem.* **1990**, *29*, 626−633.
(2) Li, N.; Petříček, V.; Coppens, P.; Landrum, J. *Acta Crystallogr., Sect. C* **1985**, *C41*, 902−905.
(3) Li, N.; Coppens, P.; Landrum, J. *Inorg. Chem.* **1988**, *27*, 482−488.
(4) Grinstaff, M. W.; Hill, M. G.; Birnbaum, E. R.; Schaefer, W. P.; Labinger, J. A.; Gray, H. B. *Inorg. Chem.* **1995**, *34*, 4896−4902.
(5) Safo, M. K.; Nesset, M. J. M.; Walker, F. A.; Debrunner, P. G.; Scheidt, W. R. *J. Am. Chem. Soc.* **1997**, *119*, 9438−9448.
(6) Polam, J. R.; Wright, J. L.; Christensen, K. A.; Walker, F. A.; Flint, H.; Winkler, H.; Grodzicki, M.; Trautwein, A. X. *J. Am. Chem. Soc.* **1996**, *118*, 5272−5276.
(7) Dolphin, D. A.; Sams, J. R.; Tsin, T. B.; Wong, K. L. *J. Am. Chem. Soc.* **1976**, *98*, 6970−6975.
(8) Grodzicki, M.; Flint, H.; Winkler, H.; Walker, F. A.; Trautwein, A. X. *J. Phys. Chem. A* **1997**, *101*, 4202−4207.
(9) Scheidt, W. R.; Chipman, D. M. *J. Am. Chem. Soc.* **1986**, *108*, 1163−1169.
(10) Mathews, F. S.; Bethge, P.; Czerwinski, E. W. *J. Mol. Biol.* **1979**, *254*, 1699−1706.
(11) Guiard, B.; Lederer, F. *J. Mol. Biol.* **1979**, *135*, 639−650.
(12) Walker, F. A.; Emrick, D.; Rivera, J. E.; Hanquet, B. J.; Buttlaire, D. H. *J. Am. Chem. Soc.* **1988**, *110*, 6234−6240.
(13) Kalsbeck, W. A.; Robertson, D. E.; Pandey, R. K.; Smith, K. M.; Dutton, P. L.; Bocian, D. F. *Biochemistry* **1996**, *35*, 3429−3438.
(14) Magalon, A.; Lemeslemeunier, D.; Rothery, R. A.; Frixon, C.; Weiner, J. H.; Blasco, F. *J. Biol. Chem.* **1997**, *272*, 25652−25658.
(15) Tsubaki, M.; Nakayama, M.; Okuyama, E.; Ichikawa, Y.; Hori, H. *J. Biol. Chem.* **1997**, *272*, 23206−23210.
(16) Rau, H. K.; Haehnel, W. *J. Am. Chem. Soc.* **1998**, *120*, 468−476.
(17) Moore, G. R.; Pettigrew, G. W. *Cytochromes c. Evolutionary, Structural and Physicochemical Aspects;* Springer-Verlag: New York, 1990.
(18) Pierrot, M.; Haser, R.; Frey, M.; Payan, F.; Astier, J. P. *J. Biol. Chem.* **1982**, *23*, 14341−14348.
(19) Higuchi, Y.; Kusunoki, M.; Yasuoka, N.; Kakudo, M.; Yagi, T. *J. Mol. Biol.* **1984**, *172*, 109−139.

10.1021/ic990178q CCC: $18.00
Published on Web 09/29/1999

that the α-amino group of Tyr-1[20] coordinates trans to His-25 in this *c*-type heme protein.[21,22] Thus, not only are amines of interest from the standpoint of delineating their coordination chemistry with iron porphyrins, but this class of ligand appears to be functionally significant in at least one hemoprotein.

The reaction of primary and secondary amines with Fe(III) porphyrins in nonaqueous solvents results in base-catalyzed one-electron reduction and concomitant dissociation of the deprotonated amine radical.[23] In the presence of excess amine, bis(amine)iron(II) complexes are obtained.[7,23−26] The mechanism of this reaction has been studied for piperidine[23] and a range of primary amines[27] in nonaqueous solvents. Only sterically unhindered alkylamines with a C−H proton adjacent to the NH or NH_2 group are capable of reducing ferric porphyrins.[27,28] Interestingly, spectroscopic studies in aqueous solution show that base-catalyzed reduction to the ferrous state is quenched, affording stable low-spin iron(III) complexes in the presence of excess amine.[29,30] Mössbauer data have been reported for a number of Fe(II) systems, including $[Fe(TPP)(Pip)_2]$,[31,32] $[Fe(OEP)(NH_3)_2]$,[7] and several $[Fe^{II}(PPIX)L_2]$ derivatives, where L is a primary or secondary amine.[33] In the latter study, frozen aqueous solutions were used and reduction was effected with sodium dithionite. Mössbauer and EPR data have also been reported for $[Fe^{III}(TPP)(NH_3)_2](CF_3SO_3)$[34] and a range of $[Fe^{III}(PPIX)L_2]$ complexes, where L is a primary, secondary, or tertiary amine.[35,36]

Despite these spectroscopic studies, there have been no systematic structural studies on bis(amine) complexes of iron porphyrins; the only X-ray structure to date is that of $[Fe(TPP)(Pip)_2]$.[37] In this paper, we present a general method for the synthesis of bis(primary amine) complexes of low-spin iron(II) porphyrins. Three complexes, $[Fe(TPP)(1\text{-}BuNH_2)_2]$, $[Fe(TPP)(BzNH_2)_2]$, and $[Fe(TPP)(PhCH_2CH_2NH_2)_2]$, have been characterized by X-ray crystallography and electronic, IR, and Mössbauer spectroscopy. The X-ray data have been used to parametrize a molecular mechanics (MM) force field for bis(amine) low-spin iron(II) porphyrins. Primary and secondary amine complexes of the type $[Fe(TPP)L_2]$, where L = 1-butylamine and piperidine, have been used for conformational analysis by MM methods to determine the optimum axial ligand orientations.

Experimental Section

General Information. All manipulations were carried out under nitrogen using a double manifold vacuum line, Schlenkware, and cannula techniques. THF and hexane were distilled over sodium/benzophenone and dichloromethane over CaH_2. Benzylamine (UniLab) was distilled over CaH_2 and stored under nitrogen over 4 Å molecular sieves. 1-Butylamine and phenethylamine (Aldrich) were distilled over CaH_2 and used immediately. H_2TPP was synthesized using published procedures.[38] [Fe(TPP)Cl] was prepared by metalation of H_2TPP with anhydrous ferrous chloride in refluxing DMF.[39] Silver triflate (Fluka) was used as received.

Electronic spectra were recorded with a Shimadzu UV-2101PC UV−vis scanning spectrophotometer using dry, degassed methylene chloride solutions in 1.0 and 0.1 cm path length cuvettes under nitrogen. IR spectra were recorded with a Shimadzu FTIR-4300 spectrometer as KBr pellets. Mössbauer spectra of polycrystalline samples of $[Fe(TPP)(1\text{-}BuNH_2)_2]$, $[Fe(TPP)(BzNH_2)_2]$, and $[Fe(TPP)(PhCH_2CH_2NH_2)_2]$ (∼30−40 mg/cm^2) in Teflon cups were recorded at selected temperatures from 5 to 300 K in a flow cryostat using a ^{57}Co(Rh) source (∼40 mCi). Doppler velocities, effected with a triangular reference waveform, were calibrated against an iron foil standard. Each spectrum was recorded in 512 channels and folded with its mirror image to give the spectral data in 256 channels.[40] The data were fitted either to the sum of two Lorentzian components on a shallow parabolic background or to the sum of two *inequivalent* quadrupole doublets to take into account a minor (∼2% in fresh samples) iron(III) impurity, the signal from which gradually increased over a period of several months. In the latter case, the line widths of each resonance comprising a given doublet were constrained to be equal. Elemental analyses (between 3 and 6 measurements per sample) were obtained with a Perkin-Elmer CHN 2400 elemental analyzer on polycrystalline samples (∼2−3 mg).

Synthesis of $[Fe(TPP)(BzNH_2)_2]$. To [Fe(TPP)Cl] (200 mg, 0.284 mmol) and silver triflate (87.6 mg, 0.341 mmol) in a two-neck 100-mL round-bottom flask under nitrogen was added 20 mL of freshly distilled THF. The solution was allowed to stir for ∼12 h at room temperature. A discrete transformation of the electronic spectrum of [Fe(TPP)Cl] was observed upon substitution of chloride ion by $CF_3SO_3^-$; the Soret, Q_v, and Q_o bands shifted from 417, 509, and 575 nm to 406, 515, and 673 nm, respectively. The solvent was removed in vacuo and the red-brown solid redissolved in dichloromethane (20 mL). The solution was filtered to remove precipitated silver chloride and transferred in four 5-mL aliquots (∼71 μmol) to four Schlenk tubes containing 600 μL (8.28 mmol) of benzylamine. In each case the

(20) Abbreviations: $1\text{-}BuNH_2$, 1-butylamine; 1-BzlIm, 1-benzylimidazole; $BzNH_2$, benzylamine; 4-CNPy, 4-cyanopyridine; 3-CNPy, 3-cyanopyridine; C_a, C_b, C_m, porphyrin α-, β-, and *meso*-carbons; C_p and C_L, phenyl and ligand carbons; $1,2\text{-}Me_2Im$, 1,2-dimethylimidazole; DMF, *N*,*N*-dimethylformamide; EFG, electric field gradient; HIm; imidazole; His, histidine; $i\text{-}PrNH_2$, isopropylamine; L, ligand in general; $\alpha\text{-}MeBzNH_2$, α-methylbenzylamine; 1-MeIm, 1-methylimidazole; 4-MeIm$^-$, 4-methylimidazole anion; 4-MePy, 4-methylpyridine; MM, molecular mechanics; N_p, porphinato nitrogen; N_{ax}, axial ligand nitrogen; OEP, 2,3,7,8,12,13,17,18-octaethylporphyrin dianion; $PhCH_2CH_2NH_2$, phenethylamine; Pip, piperidine; Py, pyridine; PPIX, di- or trianion of protoporphyrin IX; TMP, 5,10,15,20-tetramesitylporphyrin dianion; THF, tetrahydrofuran; TPP, 5,10,15,20-tetraphenylporphyrin dianion; Tyr, tyrosine; 1-VinIm, 1-vinylimidazole.

(21) Martinez, S. E.; Huang, D.; Szczepaniak, A.; Cramer, W. A.; Smith, J. L. *Structure* **1994**, *2*, 95−105.
(22) Martinez, S. E.; Huang, D.; Ponomarev, M.; Cramer, W. A.; Smith, J. L. *Protein Sci.* **1996**, *5*, 1081−1092.
(23) Del Gaudio, J.; La Mar, G. N. *J. Am. Chem. Soc.* **1978**, *100*, 1112−1119.
(24) Del Gaudio, J.; La Mar, G. N. *J. Am. Chem. Soc.* **1976**, *98*, 3014−3015.
(25) Dixon, D. W.; Kirmaier, C.; Holten, D. *J. Am. Chem. Soc.* **1985**, *107*, 808−813.
(26) The redox chemistry of several bis(amino ester) complexes of a chiral Ru(II) porphyrin in dichloromethane solution has recently been described. As with iron, the Ru(II) complexes are the most stable (Morice, C.; Lemaux, P.; Moinet, C.; Simonneaux, G. *Inorg. Chim. Acta* **1998**, *273*, 142−150).
(27) Castro, C. E.; Jamin, M.; Yokoyama, W.; Wade, R. *J. Am. Chem. Soc.* **1986**, *108*, 4179−4187.
(28) Morice, C.; Le Maux, P.; Simonneaux, G. *Inorg. Chem.* **1998**, *37*, 6100−6103.
(29) Byfield, M. P.; Pratt, J. M. *J. Chem. Soc., Chem. Commun.* **1992**, 214−215.
(30) Byfield, M. P.; Hamza, M. S. A.; Pratt, J. M. *J. Chem. Soc., Dalton Trans.* **1993**, 1641−1654.
(31) Collman, J. P.; Hoard, J. L.; Kim, N.; Lang, G.; Reed, C. A. *J. Am. Chem. Soc.* **1975**, *97*, 2676−2681.
(32) Epstein, L. M.; Straub, D. K.; Maricondi, C. *Inorg. Chem.* **1967**, *6*, 1720−1724.
(33) Ahmet, M. T.; Al-Jaff, G.; Silver, J.; Wilson, M. T. *Inorg. Chim. Acta* **1991**, *183*, 43−49.
(34) Kim, Y. O.; Goff, H. M. *Inorg. Chem.* **1990**, *29*, 3907−3908.
(35) Marsh, P. J.; Silver, J.; Symons, M. C. R.; Taiwo, F. A. *J. Chem. Soc., Dalton Trans.* **1996**, 2361−2369.
(36) Brautigan, D. L.; Feinberg, B. A.; Hoffman, B. M.; Margoliash, E.; Peisach, J.; Blumberg, W. E. *J. Biol. Chem.* **1977**, *252*, 574−582.
(37) Radonovich, L. J.; Bloom, A.; Hoard, J. L. *J. Am. Chem. Soc.* **1972**, *94*, 2073−2078.
(38) Barnett, G. H.; Hudson, M. F.; Smith, K. M. *J. Chem. Soc., Perkin Trans. 1* **1975**, 1401−1403.
(39) Adler, A. D.; Longo, F. R.; Kampas, F.; Kim, J. *J. Inorg. Nucl. Chem.* **1970**, *32*, 2443.
(40) The data folding procedure eliminates geometrical effects and gives a flat baseline. The transmission integral routine of the program NORMOS (Wissenschafteliche Elektronik GmbH (WISSEL), Starnberg, Germany) was used to effect all data transforms.

solution changed color from brown to deep red on swirling, consistent with reduction of the metal to the ferrous state.[27] The solutions were layered with hexane; X-ray-quality crystals were observed after 4 days. The deep red crystals of [Fe(TPP)($BzNH_2$)$_2$] were collected by filtration and washed with hexane to remove colorless crystals of benzylamine. Isolated yield: 55 mg, 22%. Anal. Calcd for $C_{58}H_{46}N_6Fe$: C, 78.91; H, 5.25; N, 9.52. Found: C, 77.25; H, 4.56; N, 9.21. IR (KBr pellet): 1535 cm^{-1} (m, $\delta(NH_2)$), 874 cm^{-1} (w, $\rho_w(NH_2)$). UV−vis (CH_2Cl_2) [λ_{max}, nm (ϵ, M^{-1} cm^{-1})]: 425 (267 × 10^3), 494 (4.42 × 10^3), 531 (21.3 × 10^3), 562 (5.25 × 10^3).

Synthesis of [Fe(TPP)(1-$BuNH_2$)$_2$]. To [Fe(TPP)Cl] (150 mg, 0.213 mmol) and silver triflate (65.7 mg, 0.256 mmol) in a two-neck 100-mL round bottom flask under nitrogen was added 20 mL of freshly distilled THF. The solution was stirred for ∼15 h at room temperature prior to removing the solvent in vacuo. The red-brown solid was redissolved in dichloromethane (20 mL) and cannula-filtered in four aliquots (∼5 mL, 53 μmol of [Fe(TPP)(OSO_2CF_3)]) into four Schlenk tubes, each containing 600 μL (6.07 mmol) of 1-butylamine. The solutions changed color from red-brown to deep red on swirling; each was layered with hexane and set aside for crystallization. X-ray-quality crystals were isolated after 4 days by filtration and washed with hexane. Isolated yield: 84.5 mg, 49%. Anal. Calcd for $C_{52}H_{50}N_6Fe$: C, 76.65; H, 6.19; N, 10.32. Found: C, 76.37; H, 5.98; N, 10.51. IR (KBr pellet): 3381 cm^{-1} (m, ν(N−H)), 1537 cm^{-1} (m, $\delta(NH_2)$). UV−vis (CH_2Cl_2) [λ_{max}, nm (ϵ, M^{-1} cm^{-1})]: 426 (235 × 10^3), 496 (4.41 × 10^3), 532 (19.8 × 10^3), 563 (5.28 × 10^3).

Synthesis of [Fe(TPP)(PhCH$_2$CH$_2$NH$_2$)$_2$]. To [Fe(TPP)Cl] (147 mg, 0.209 mmol) and silver triflate (64.9 mg, 0.253 mmol) in a two-neck 100-mL round-bottom flask under nitrogen was added 40 mL of freshly distilled THF. The solution was stirred for 12 h at room temperature prior to removing the solvent in vacuo. The red-brown solid was redissolved in dichloromethane (∼16 mL) and cannula-filtered into a 50-mL two-neck round bottom flask to which 1.3 mL (10.5 mmol) of freshly-distilled $PhCH_2CH_2NH_2$ was added under nitrogen. *Caution! Phenethylamine is a toxic (possible nervous system sensitizer), corrosive compound and should be handled under strictly anaerobic conditions in a fume hood*. The solution turned from red-brown to deep red on swirling. The reaction mixture was transferred to five 25-mL Schlenk tubes (∼3 mL aliquots) and layered with hexane. X-ray-quality crystals were isolated after 4 days by filtration and washed with 96% ethanol to remove colorless crystals of $PhCH_2CH_2NH_2$. Isolated yield: 109 mg, 57%. Anal. Calcd for $C_{60}H_{50}N_6Fe$: C, 79.11; H, 5.53; N, 9.27. Found: C, 78.79; H, 5.45; N, 9.66. IR (KBr pellet): 1537 cm^{-1} (m, $\delta(NH_2)$). UV−vis (CH_2Cl_2) [λ_{max}, nm (ϵ, M^{-1} cm^{-1})]: 426 (274 × 10^3), 531 (23.3 × 10^3), 562 (6.35 × 10^3).

Synthesis and Attempted Crystallization of [Fe(TPP)(*R*-[+]-α-MeBzNH$_2$)$_2$]. The reaction was carried out as above with [Fe(TPP)Cl] (150 mg, 0.213 mmol), silver triflate (62 mg, 0.24 mmol), and excess *R*-[+]-α-methylbenzylamine (∼2 mL). The solution turned deep red following the addition of the amine. The visible spectrum in CH_2Cl_2 showed bands at 530 and 564 nm, consistent with reduction of the metal to the ferrous state. Attempts to grow single crystals of [Fe(TPP)(*R*-[+]-α-MeBzNH$_2$)$_2$] from several solvents were unsuccessful; crystals of [Fe(TPP)]$_2$O were obtained after prolonged periods (>7 days).

Synthesis and Attempted Crystallization of [Fe(TPP)(*i*-PrNH$_2$)$_2$]. The reaction was carried out as before with [Fe(TPP)Cl] (142 mg, 0.202 mmol), silver triflate (68.5 mg, 0.267 mmol), and excess isopropylamine (∼4 mL). Reduction of the metal to the ferrous state was observed on swirling the reaction mixture. Attempts to grow single crystals of [Fe(TPP)(*i*-PrNH$_2$)$_2$] from CH_2Cl_2/hexane were unsuccessful.

X-ray Structure Determinations. Crystals of [Fe(TPP)(1-$BuNH_2$)$_2$], [Fe(TPP)($BzNH_2$)$_2$], and [Fe(TPP)($PhCH_2CH_2NH_2$)$_2$] were purple-black six-sided (0.43 × 0.35 × 0.18 mm), dark red eight-sided (0.35 × 0.30 × 0.15 mm), and dark red seven-sided (0.62 × 0.27 × 0.27 mm) rhombs, respectively. X-ray diffraction data were collected on an Enraf-Nonius CAD4 diffractometer at 293(2) K with graphite-monochromated Mo Kα radiation ($\bar{\lambda}$ = 0.717 03 Å). Intensities of all reflections were reduced using Lorentz and polarization correction factors; the data were also corrected for absorption ([Fe(TPP)(1-$BuNH_2$)$_2$], μ = 0.390 mm^{-1}; [Fe(TPP)($BzNH_2$)$_2$], μ = 0.387 mm^{-1}; [Fe(TPP)($PhCH_2CH_2NH_2$)$_2$], μ = 0.374 mm^{-1}) using a semiempirical absorption correction based on ψ scans (360°) of 9 reflections with χ > 75°.[41] A total of 4840, 6878, and 3782 observed reflections ($F_o \geq 2.0\sigma(F_o)$) were collected and averaged to 3786, 6159, and 3210 unique data for [Fe(TPP)(1-$BuNH_2$)$_2$], [Fe(TPP)($BzNH_2$)$_2$], and [Fe(TPP)($PhCH_2CH_2NH_2$)$_2$], respectively.

The structures of the three low-spin iron(II) porphyrins were solved in the triclinic space group $P\bar{1}$ with the Patterson vector superposition procedure of SHELXS-93[42] as implemented in the SHELX-97[43a] suite of programs. The iron atom of [Fe(TPP)($BzNH_2$)$_2$] was located at a general position; the iron atoms of [Fe(TPP)(1-$BuNH_2$)$_2$] and [Fe(TPP)($PhCH_2CH_2NH_2$)$_2$] were located at a center of inversion (the unit cell origin). Difference Fourier syntheses were used to locate the remaining non-hydrogen atoms. The structures were refined anisotropically against F^2 with SHELXL-97.[43a] In each case, a final difference Fourier synthesis led to location of all hydrogens atoms, including those of the coordinated amine nitrogens. All were included as idealized contributors in the least-squares process with standard SHELXL-97 idealization parameters. The final refinements of [Fe(TPP)(1-$BuNH_2$)$_2$], [Fe(TPP)($BzNH_2$)$_2$], and [Fe(TPP)($PhCH_2CH_2NH_2$)$_2$] converged to the discrepancy indices listed below. The maximum (and minimum) electron densities on the final difference Fourier maps of [Fe(TPP)(1-$BuNH_2$)$_2$], [Fe(TPP)($BzNH_2$)$_2$], and [Fe(TPP)($PhCH_2CH_2NH_2$)$_2$] were 0.292 (−0.298), 0.379 (−0.312), and 0.216 (−0.253) e/Å^3, respectively.

Complete crystallographic details, fractional atomic coordinates for all non-hydrogen atoms, anisotropic thermal parameters, fixed hydrogen atom coordinates, bond lengths, bond angles, and dihedral angles for [Fe(TPP)(1-$BuNH_2$)$_2$], [Fe(TPP)($BzNH_2$)$_2$], and [Fe(TPP)($PhCH_2CH_2NH_2$)$_2$] are given in the Supporting Information (Tables S1−S21).

[Fe(TPP)(1-$BuNH_2$)$_2$]: $C_{52}H_{50}FeN_6$, fw = 814.83 amu, a = 10.118(10) Å, b = 11.086(14) Å, c = 11.205(3) Å, α = 94.15(4)°, β = 105.62(5)°, γ = 113.88(6)°, V = 1083.1(18) Å^3, triclinic, $P\bar{1}$, Z = 1, D_c = 1.249 g cm^{-3}, μ = 0.391 mm^{-1}, T = 293(2) K, R_1 (wR_2)[44] = 0.0401 (0.0985) for 3193 unique data with $I > 2\sigma(I)$, R_1 (wR_2) = 0.0541 (0.1108) for all 3786 data (R_{int} = 0.0176).

[Fe(TPP)($BzNH_2$)$_2$]: $C_{58}H_{46}FeN_6$, fw = 882.86 amu, a = 11.742(5) Å, b = 12.348(6) Å, c = 17.404(4) Å, α = 97.69(3)°, β = 101.97(3)°, γ = 112.16(4)°, V = 2222.7(15) Å^3, triclinic, $P\bar{1}$, Z = 2, D_c = 1.319 g cm^{-3}, μ = 0.387 mm^{-1}, T = 293(2) K, R_1 (wR_2)[44] 0.0436 (0.1004) for 4702 unique data with $I > 2\sigma(I)$, R_1 (wR_2) = 0.0710 (0.1226) for all 6159 data (R_{int} = 0.0194).

[Fe(TPP)($PhCH_2CH_2NH_2$)$_2$]: $C_{60}H_{50}FeN_6$, fw = 910.91 amu, a = 10.9625(16) Å, b = 11.203(3) Å, c = 11.299(4) Å, α = 75.23(3)°, β = 89.12(2)°, γ = 60.419(17)°, V = 1156.8(5) Å^3, triclinic, $P\bar{1}$, Z = 1, D_c = 1.308 g cm^{-3}, μ = 0.374 mm^{-1}, T = 293(2) K, R_1 (wR_2)[44] = 0.0319 (0.0806) for 2859 unique data with $I > 2\sigma(I)$, R_1 (wR_2) = 0.0405 (0.0890) for all 3210 data (R_{int} = 0.0122).

Molecular Mechanics Calculations. These were performed on an IBM-compatible computer with HyperChem 5.02 (MM+ force field).[45] Porphyrin force field parameters were taken from our published set

(41) North, A. C. T.; Phillips, D. C.; Mathews, F. S. *Acta Crystallogr., Sect. A* **1968**, *A24*, 351.
(42) Sheldrick, G. M.; Dauter, Z.; Wilson, K. S.; Hope, H.; Sieker, L. C. *Acta Crystallogr., Sect. D* **1993**, *D49*, 18−23.
(43) (a) SHELX-97: Sheldrick, G. M. *J. Appl. Crystallogr.*, manuscript in preparation. (b) Oscail and ORTEX V7e 1999: P. McArdle, Crystallography Centre, Chemistry Department, NUI Galway, Ireland (McArdle, P. *J. Appl. Crystallogr.* **1995**, *28*, 65). (c) Ortep-3 for Windows V1.01β: Louis J. Farrugia, Department of Chemistry, University of Glasgow, Glasgow G12 8QQ, Scotland, 1998. (d) ORTEP III: Burnett, M. N.; Johnson, C. K. Oak Ridge National Laboratory Report ORNL-6895, 1996.
(44) $R_1 = \sum||F_o| - |F_c||/\sum|F_o|$ and $wR_2 = \{\sum[w(F_o^2 - F_c^2)^2]/\sum[wF_o^4]\}^{1/2}$. R factors R_1 are based on F, with F set to zero for negative F^2. The criterion of $F^2 > 2\sigma(F^2)$ was used only for calculating R_1. R factors based on F^2 (wR_2) are statistically about twice as large as those based on F.
(45) HyperChem 5.02: Hypercube, Inc., 1115 NW 4th St., Gainsville, FL 32601-4256. Other programs used in this study: (a) AXUM, Technical Graphics and Data Analysis, V. 3.0. TriMetrix Inc., 444 NE Ravenna Boulevard, Suite 210, Seattle, WA 98115. (b) Corel Draw 8. Corel Corp., 1600 Carling Ave., Ottawa, Ontario, Canada K1Z 8R7.

for low-spin iron(III) porphyrins;[45−48] these were used in conjunction with new bond stretching, angle bending, and dihedral angle parameters for bis(amine) low-spin iron(II) derivatives.[49] Input structures were either the X-ray structures of [Fe(TPP)(1-$BuNH_2)_2$], [Fe(TPP)($BzNH_2)_2$], [Fe(TPP)($PhCH_2CH_2NH_2)_2$], and [Fe(TPP)($Pip)_2$][37] (orthogonalized coordinates) or idealized structures with planar core conformations. A root mean square gradient termination cutoff of 0.004 kcal/(Å mol) was used for geometry optimization with the Polak−Ribiere conjugate gradient algorithm. A dielectric constant of 1.5 D was employed for all calculations. The vacuum dielectric constant (1.0 D) was not used because even in the gas phase some screening of intramolecular dipole−dipole interactions occurs.[50,51] Partial atomic charges were not included in the calculations.[48,52,53] Comparison of the energy-minimized and X-ray structures of [Fe(TPP)(1-$BuNH_2)_2$], [Fe(TPP)($BzNH_2)_2$], [Fe(TPP)($PhCH_2CH_2NH_2)_2$], and [Fe(TPP)($Pip)_2$] gave acceptable rmsd's (bond lengths, bond angles, and dihedral angles).

A crystal packing calculation for [Fe(TPP)(1-$BuNH_2)_2$] was used to evaluate the role of intermolecular nonbonded interactions in perturbing the orientations of the porphyrin phenyl groups and axial ligands in this class of compounds. Specifically, a lattice subset comprising 15 molecules (30 asymmetric units) was generated from the fractional coordinates of the X-ray structure. The centermost molecule, surrounded by 14 invariant neighboring molecules, was chosen for geometry optimization with fixed Fe(II) coordinates to maintain the metal ion at its special position within the lattice. No other restraints were necessary.

Conformational surfaces for [Fe(TPP)(1-$BuNH_2)_2$] and [Fe(TPP)-($Pip)_2$] were calculated by counter-rotating the axial ligands from 0 to 360° (for both ϕ_1 and ϕ_2) in 10° increments, producing a total of 37^2 starting conformations for refinement. Dihedral angles involving a porphyrin nitrogen atom, the Fe(II) ion, a coordinated axial nitrogen, and a ligand α-carbon ($N_p-Fe-N_{ax}-C_L$, ϕ) were used to define the axial ligand orientations.[54] A maximum of 2000 least-squares cycles with a root mean square gradient termination cutoff of 0.01 kcal/(Å mol) was used for geometry optimization with the Polak−Ribiere conjugate gradient algorithm.

Results

Crystal Structures. The molecular structures and numbering schemes for the crystallographically unique atoms of [Fe(TPP)-(1-$BuNH_2)_2$], [Fe(TPP)($BzNH_2)_2$], and [Fe(TPP)($PhCH_2CH_2$-$NH_2)_2$] are shown in the ORTEP plots of Figure 1. [Fe(TPP)(1-$BuNH_2)_2$] and [Fe(TPP)($PhCH_2CH_2NH_2)_2$] have crystallographically required inversion symmetry, as evidenced by the anti arrangement of the axial ligands in each case. The α-CH_2 groups of the 1-butylamine ligands of [Fe(TPP)(1-$BuNH_2)_2$] are positioned approximately over the closest Fe−N_p bonds; the dihedral angle N(1)−Fe−N(3)−C(31) measures 15.2(3)°. The phenethylamine ligands of [Fe(TPP)($PhCH_2CH_2NH_2)_2$] are positioned directly over the closest Fe−N_p bonds with a dihedral angle to the α-CH_2 groups, N(1)−Fe−N(3)−C(31), of 0.24-(18)°. In contrast, [Fe(TPP)($BzNH_2)_2$] lacks inversion symmetry; the α-CH_2 groups of the two axial benzylamine ligands are positioned one approximately over the nearest Fe−N_p bond and the other approximately over the nearest bisector of a *cis*-N_p−Fe−N_p angle. The dihedral angles defining the ligand orientations relative to the porphyrin core, N(3)−Fe−N(5)−C(51) and N(4)−Fe−N(6)−C(61), measure 18.2(4) and 30.1(4)°, respectively. The *meso*-phenyl groups of [Fe(TPP)(1-$BuNH_2)_2$], [Fe-(TPP)($BzNH_2)_2$], and [Fe(TPP)($PhCH_2CH_2NH_2)_2$] are slightly to moderately tilted from the heme normal; individual $C_a-C_m-C_p-C_p$ angles range from 70.8 to 89.8° (Table 1).

Formal diagrams of the porphinato cores of [Fe(TPP)(1-$BuNH_2)_2$], [Fe(TPP)($BzNH_2)_2$], and [Fe(TPP)($PhCH_2CH_2NH_2)_2$] are shown in Figure 2; the perpendicular displacement of each crystallographically unique atom from the 24-atom porphyrin mean plane and the averaged values of the chemically unique bond distances and angles are displayed in each case. The individual Fe−N_p bond distances and orientations of the axial ligands relative to the Fe−N_p bonds are also shown. The porphyrin core of each derivative is approximately planar; the individual atomic displacements are all <0.13 Å. With the exception of the required inversion symmetry for [Fe(TPP)(1-$BuNH_2)_2$] and [Fe(TPP)($PhCH_2CH_2NH_2)_2$], no systematic pattern of atomic displacements leading to a well-defined symmetry is evident.

The average Fe−N_p bond lengths for [Fe(TPP)(1-$BuNH_2)_2$], [Fe(TPP)($BzNH_2)_2$], and [Fe(TPP)($PhCH_2CH_2NH_2)_2$] are 1.989-(1), 1.992(4), and 1.989(4) Å, respectively. These are somewhat shorter than the Fe−N_p distances of other bis(N-donor) low-spin iron(II) porphyrins.[1−3,5,55] The average Fe−N_{ax} bond length for [Fe(TPP)($BzNH_2)_2$] is 2.043(3) Å; the unique Fe−N_{ax} bond lengths of [Fe(TPP)(1-$BuNH_2)_2$] and [Fe(TPP)($PhCH_2CH_2$-$NH_2)_2$] are 2.039(3) and 2.028(2) Å, respectively. The N_{ax}−Fe−N_{ax} angles are 180.0° for [Fe(TPP)(1-$BuNH_2)_2$] and [Fe-(TPP)($PhCH_2CH_2NH_2)_2$], consistent with the crystallographically required inversion symmetry. In contrast, the N_{ax}−Fe−N_{ax} angle for [Fe(TPP)($BzNH_2)_2$] is 176.2(1)°. The N_p−Fe−N_{ax} angles span the range 88.1(1)−91.9(1)° for [Fe(TPP)(1-$BuNH_2)_2$], 87.3-(1)−92.0(1)° for [Fe(TPP)($BzNH_2)_2$], and 86.3(7)−93.8(7)° for [Fe(TPP)($PhCH_2CH_2NH_2)_2$], consistent with a modest off-axis tilt for each alkylamine ligand. Selected bond lengths, bond angles, and dihedral angles for [Fe(TPP)(1-$BuNH_2)_2$], [Fe(TPP)-($BzNH_2)_2$], and [Fe(TPP)($PhCH_2CH_2NH_2)_2$] are given in Table 1; complete listings of structural data are given in the Supporting Information.

(46) Munro, O. Q.; Bradley, J. C.; Hancock, R. D.; Marques, H. M.; Marsicano, F.; Wade, P. W. *J. Am. Chem. Soc.* **1992**, *114*, 7218−7230.
(47) Marques, H. M.; Munro, O. Q.; Grimmer, N. E.; Levendis, D. C.; Marsicano, F.; Pattrick, G.; Markoulides, T. *J. Chem. Soc., Faraday Trans.* **1995**, *91*, 1741−1749.
(48) Munro, O. Q.; Marques, H. M.; Debrunner, P. G.; Mohanrao, K.; Scheidt, W. R. *J. Am. Chem. Soc.* **1995**, *117*, 935−954.
(49) The following parameters were developed for bis(amine) low-spin Fe(II) porphyrins using the X-ray structures of [Fe(TPP)(1-$BuNH_2)_2$], [Fe(TPP)($BzNH_2)_2$], [Fe(TPP)($PhCH_2CH_2NH_2)_2$], and [Fe(TPP)-($Pip)_2$][37] for parametrization. Bond deformation: bond, k_s (mdyn Å^{-1}), l_0 (Å); N_p−Fe(II), 1.850, 1.922; N_{ax}−Fe(II), 1.900, 2.002. Bond angle deformation: angle, k_θ (mdyn Å rad^{-2}), θ_0 (deg); *trans*-N_p−Fe(II)−N_p, 0.005, 180.0; *cis*-N_p−Fe(II)−N_p, 0.200, 90.0; N_p−Fe(II)−N_{ax}, 0.300, 90.0; N_{ax}−Fe(II)−N_{ax}, 1.000, 180.0; C_a-N_p−Fe(II), 0.700, 126.8; C(sp^3)−N_{ax}−Fe(II), 0.400, 120.0; H−N_{ax}−Fe(II), 0.400, 109.47. Dihedral angle deformation: dihedral angle, V_1, V_2, V_3 (kcal mol^{-1}); C_a-N_p−Fe(II)−N_p (N_p−Fe(II)−N_p trans), 0.000, 0.000, 0.000; C_a-N_p−Fe(II)−N_p (N_p−Fe(II)−N_p cis), 0.000, 0.100, 0.000; Fe(II)−N_{ax}−C(sp^3)−H, 0.000, 0.000, 0.520; Fe(II)−N_{ax}−C(sp^3)−C(sp^3), −0.200, 0.730, 0.800; Fe(II)−N_{ax}−C(sp^3)−C(sp^2), 0.000, 0.000, 0.000; N_p−Fe(II)−N_{ax}−C(sp^3), 0.000, 0.000, 0.000; N_p−Fe(II)−N_{ax}−H, 0.000, 0.000, 0.000; N_{ax}−Fe(II)−N_{ax}−H, 0.000, 0.000, 0.000; C(sp^2)−C(sp^2)−C(sp^3)−N_{ax}, 0.000, 0.000, 0.000.
(50) (a) Allinger, N. L. *J. Am. Chem. Soc.* **1977**, *99*, 8127. (b) Allinger, N. L.; Yuh, Y. MM2(87). Distributed to academic users by QCPE, under special agreement with Molecular Design Ltd., San Leandro, CA. (c) Sprague, J. T.; Tai, J. C.; Young, Y.; Allinger, N. L. *J. Comput. Chem.* **1987**, *8*, 581.
(51) Jensen, F. *Introduction to Computational Chemistry*; Wiley: New York, 1999; pp 23−25.
(52) Shelnutt, J. A.; Medforth, C. J.; Berber, M. D.; Barkigia, K. M.; Smith, K. M. *J. Am. Chem. Soc.* **1991**, *113*, 4077−4087.
(53) The force field includes the standard MM2[50] bond dipoles for the C−C and C−N bonds. All M−L bond dipoles have an assigned value of zero.
(54) HyperChem uses stiff restraining force constants (V_2 = 250 kcal/mol) to fix the selected dihedral angles during geometry optimization. These are removed after convergence, and the total steric energy is determined by a single point calculation with the normal force constants for all dihedral angles in the molecule.
(55) The structures of [Fe(TMP)(4-CNPy)$_2$], [Fe(TMP)(3-CNPy)$_2$], and Fe(TMP)(4-MePy)$_2$] have mean Fe−N_p distances of 1.992(1), 1.988(0), and 1.996(0) Å, respectively.[5]

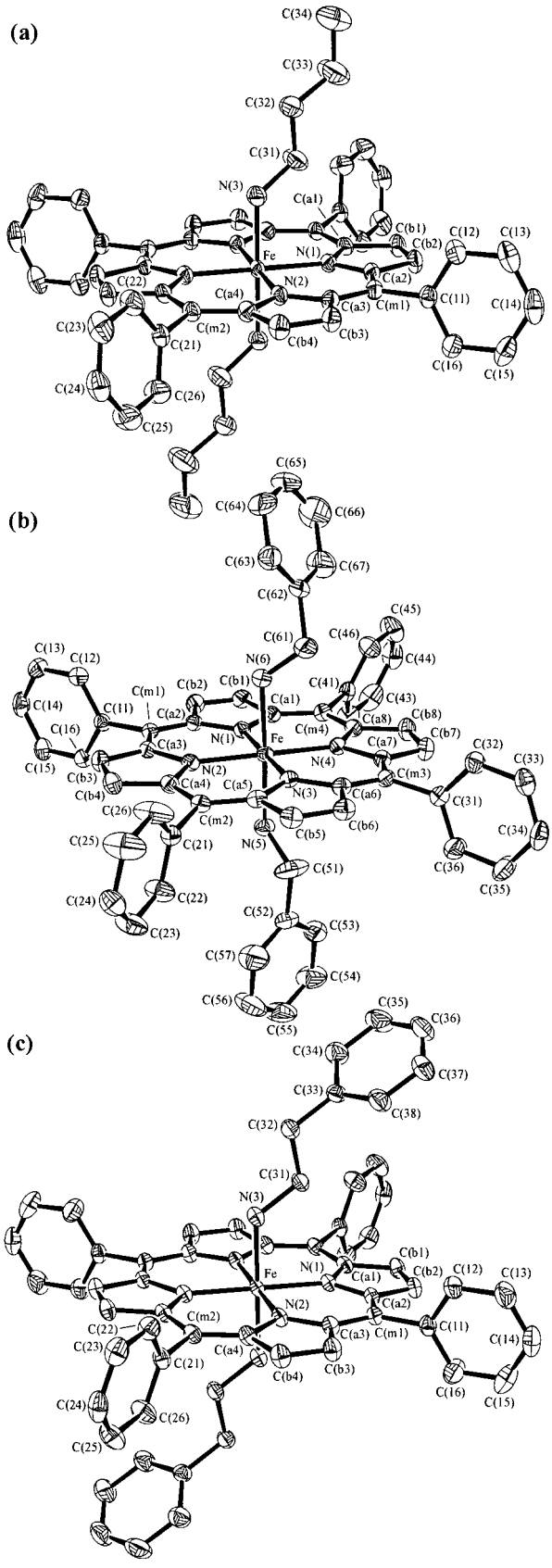

Figure 1. Labeled ORTEP plots (ORTEP-3)[43c] of the X-ray structures of (a) [Fe(TPP)(1-BuNH$_2$)$_2$], (b) [Fe(TPP)(BzNH$_2$)$_2$], and (c) [Fe(TPP)(PhCH$_2$CH$_2$NH$_2$)$_2$]. Thermal ellipsoids are drawn at the 30% probability level. Hydrogen atoms have been omitted for clarity.

Electronic and Mössbauer Spectroscopy. The electronic spectra of [Fe(TPP)(1-BuNH$_2$)$_2$], [Fe(TPP)(BzNH$_2$)$_2$], and [Fe(TPP)(PhCH$_2$CH$_2$NH$_2$)$_2$] are similar (Figure 3); the Soret, Q_v, and Q_o bands occur at ~426, ~532, and ~562 nm, respectively. The wavelengths and intensity pattern of the Q-bands (Q_o less intense than Q_v, both sharp) are consistent with other low-spin iron(II) porphyrins with *meso*-aryl substituents and two axial N-donor ligands.[1] The visible and UV bands show a systematic increase in intensity from [Fe(TPP)(1-BuNH$_2$)$_2$] to [Fe(TPP)(PhCH$_2$CH$_2$NH$_2$)$_2$]; this is particularly evident for the Q_v band at 532 nm. Because of the possible lability of the six-coordinate iron(II) species in solution, excess alkylamine ligand was used in each case to ensure that the spectrum of the six-coordinate derivative was obtained. Importantly, the IR spectra of all three crystalline samples used to prepare solutions for UV−visible spectroscopy showed no bands at 892 and 878 cm^{-1} due to possible contamination by the stable iron(III) hydrolysis product [Fe(TPP)]$_2$O.[56] Bands in the visible spectrum due to this species (572 and 612 nm)[56] are also absent.

Zero-field Mössbauer spectra recorded as a function of temperature for [Fe(TPP)(BzNH$_2$)$_2$] are shown in Figure 4; the spectra for [Fe(TPP)(1-BuNH$_2$)$_2$] and [Fe(TPP)(PhCH$_2$CH$_2$NH$_2$)$_2$] (not shown) are similar. Quadrupole splittings, isomer shifts, and line widths at different temperatures for the three primary amine complexes are given in Table 2 along with data for related systems.[7,32,33] The isomer shifts, δ, of the primary amine complexes range from 0.393(1) to 0.493(1) mm/s and show a weak temperature dependence due to the second-order Doppler shift.[57] The quadrupole splittings, ΔE_Q, for the three primary amine complexes range from 1.144(6) to 1.204(3) mm/s and also increase marginally (~0−0.04 mm/s) with temperature. The spectra were adequately fitted with equivalent quadrupole doublet component line widths, consistent with normal relaxation behavior for this class of low-spin iron(II) porphyrinates.[57] However, the polycrystalline samples were not indefinitely stable even when stored in a desiccator. Slow air-oxidation was observed over a period of several months, particularly for [Fe(TPP)(BzNH$_2$)$_2$], the Mössbauer spectrum of which showed an increase in signal intensity (2−21%) from a high-spin iron(III) oxidation product (δ = 0.353(6) mm/s, ΔE_Q = 0.64(1) mm/s).

Molecular Mechanics Calculations. MM-calculated and crystallographically observed bond distances, bond angles, and dihedral angles for [Fe(TPP)(1-BuNH$_2$)$_2$], [Fe(TPP)(BzNH$_2$)$_2$], [Fe(TPP)(PhCH$_2$CH$_2$NH$_2$)$_2$], and [Fe(TPP)(Pip)$_2$][37] are compared in Tables S22−S28 of the Supporting Information. The average difference between the calculated and observed structures is 0.011(11) Å (bond distances), 0.7(1.0)° (bond angles), and 1.7(1.7)° (dihedral angles). This level of agreement exceeds that obtained previously with our force field for S_4-ruffled and planar bis(imidazole)iron(III) porphyrins.[48]

Figure 5 compares the calculated (gas phase) and crystallographically observed structures of [Fe(TPP)(1-BuNH$_2$)$_2$], [Fe(TPP)(BzNH$_2$)$_2$], [Fe(TPP)(PhCH$_2$CH$_2$NH$_2$)$_2$], and [Fe(TPP)(Pip)$_2$].[58] The porphyrin core conformations and coordination sphere geometries of the X-ray structures are well modeled in the calculated structures (rmsd's < 0.08 Å). The largest deviations are for the axial ligand and porphyrin phenyl groups. The *meso*-phenyl group orientations (C_a−C_m−C_p−C_p) average 90.0° for both the X-ray and calculated structures. However,

(56) Fleischer, E. B.; Srivastava, T. S. *J. Am. Chem. Soc.* **1969**, *91*, 2403−2405.
(57) Debrunner, P. G. In *Iron Porphyrins*; Physical Bioinorganic Chemistry Series; Lever, A. B. P., Gray, H. B., Eds.; Addison-Wesley: Reading, MA, 1989; Part 3, pp 139−234.
(58) Each calculated structure has been fitted to the X-ray structure by least-squares minimization of the positional differences between the iron, porphyrin core, and axial nitrogen atoms.

Table 1. Selected Bond Lengths, Bond Angles, and Dihedral Angles for [Fe(TPP)(1-$BuNH_2)_2$], [Fe(TPP)($BzNH_2)_2$], and [Fe(TPP)($PhCH_2CH_2NH_2)_2$][a]

(A) Bond Lengths

[Fe(TPP)($BzNH_2)_2$]		[Fe(TPP)(1-$BuNH_2)_2$]/ [Fe(TPP)($PhCH_2CH_2NH_2)_2$]	
bond	length (Å)	bond	length (Å)
Fe−N(1)	1.993(3)	Fe−N(1)	1.988(3)[b]
Fe−N(2)	1.995(3)	Fe−N(2)	1.989(2)[b]
Fe−N(3)	1.986(3)	Fe−N(3)	2.039(3)[b]
Fe−N(4)	1.994(3)	Fe−N(1)	1.9920(18)[c]
Fe−N(5)	2.045(3)	Fe−N(2)	1.9858(18)[c]
Fe−N(6)	2.041(3)	Fe−N(3)	2.0278(18)[c]

(B) Bond Angles

[Fe(TPP)($BzNH_2)_2$]		[Fe(TPP)(1-$BuNH_2)_2$]/ [Fe(TPP)($PhCH_2CH_2NH_2)_2$]	
angle	deg	angle	deg
N(1)−Fe−N(2)	89.73(12)	N(1)[d]−Fe−N(2)[d]	90.22(10)[b]
N(1)−Fe−N(3)	179.32(11)	N(1)−Fe−N(2)[d]	89.78(10)[b]
N(1)−Fe−N(4)	90.05(12)	N(1)[d]−Fe−N(3)	88.06(12)[b]
N(1)−Fe−N(5)	89.33(13)	N(1)−Fe−N(3)	91.94(12)[b]
N(1)−Fe−N(6)	87.34(13)	N(2)[d]−Fe−N(3)	90.75(10)
N(3)−Fe−N(2)	90.07(12)	N(2)−Fe−N(3)	89.25(10)[b]
N(3)−Fe−N(4)	90.15(12)	N(1)[d]−Fe−N(1)	180.0[b,c]
N(3)−Fe−N(5)	91.32(12)	N(2)[d]−Fe−N(2)	180.0[b,c]
N(3)−Fe−N(6)	92.01(13)	N(3)[d]−Fe−N(3)	180.0[b,c]
N(4)−Fe−N(2)	179.68(12)	N(2)[d]−Fe−N(1)	90.09(7)[c]
N(4)−Fe−N(5)	90.08(12)	N(2)−Fe−N(1)	89.91(7)[c]
N(4)−Fe−N(6)	91.71(12)	N(2)[d]−Fe−N(3)	89.84(7)[c]
N(5)−Fe−N(2)	89.69(12)	N(2)−Fe−N(3)	90.16(7)[c]
N(6)−Fe−N(2)	88.51(12)	N(1)−Fe−N(3)	93.75(7)[c]
N(6)−Fe−N(5)	176.22(13)	N(1)[d]−Fe−N(3)	86.25(7)[c]

(C) Dihedral Angles

[Fe(TPP)($BzNH_2)_2$]		[Fe(TPP)(1-$BuNH_2)_2$]/ [Fe(TPP)($PhCH_2CH_2NH_2)_2$]	
angle	deg	angle	deg
N(1)−Fe−N(5)−C(51)	162.0(4)	N(1)[d]−Fe−N(3)−C(31)	−164.8(3)[b]
N(2)−Fe−N(5)−C(51)	−108.2(4)	N(1)−Fe−N(3)−C(31)	15.2(3)[b]
N(3)−Fe−N(5)−C(51)	−18.2(4)	N(2)[d]−Fe−N(3)−C(31)	−74.6(3)[b]
N(4)−Fe−N(5)−C(51)	72.0(4)	N(2)−Fe−N(3)−C(31)	105.4(3)[b]
N(1)−Fe−N(6)−C(61)	−120.1(4)	N(2)[d]−Fe−N(3)−C(31)	−89.84(18)[c]
N(2)−Fe−N(6)−C(61)	150.1(4)	N(2)−Fe−N(3)−C(31)	90.16(18)[c]
N(3)−Fe−N(6)−C(61)	60.1(4)	N(1)−Fe−N(3)−C(31)	0.24(18)[c]
N(4)−Fe−N(6)−C(61)	−30.1(4)	N(1)[d]−Fe−N(3)−C(31)	−179.76(18)[c]
C(a2)−C(m1)−C(11)−C(12)	−92.0(4)	C(a2)−C(m1)−C(11)−C(12)	78.6(3)[b]
C(a3)−C(m1)−C(11)−C(12)	90.2(4)	C(a3)−C(m1)−C(11)−C(12)	−99.4(3)[b]
C(a4)−C(m2)−C(21)−C(22)	83.5(5)	C(a1)[d]−C(m2)−C(21)−C(22)	−76.6(3)[b]
C(a5)−C(m2)−C(21)−C(22)	−93.2(5)	C(a4)−C(m2)−C(21)−C(22)	105.7(3)[b]
C(a6)−C(m3)−C(31)−C(32)	−92.2(4)	C(a2)−C(m1)−C(11)−C(12)	93.2(3)[c]
C(a7)−C(m3)−C(31)−C(32)	92.3(5)	C(a3)−C(m1)−C(11)−C(12)	−85.2(3)[c]
C(a1)−C(m4)−C(41)−C(42)	−72.6(5)	C(a4)−C(m2)−C(21)−C(22)	86.7(3)[c]
C(a8)−C(m4)−C(41)−C(42)	109.2(4)	C(a1)[d]−C(m2)−C(21)−C(22)	−94.2(3)[c]

[a] The estimated standard deviations of the least significant digits are given in parentheses. [b] [Fe(TPP)(1-$BuNH_2)_2$]. [c] [Fe(TPP)($PhCH_2CH_2NH_2)_2$]. [d] Symmetry equivalent (−*x*, −*y*, −*z*).

each experimental mean has a large associated esd due to individual orientations which deviate from 90° by as much as 26° in the case of [Fe(TPP)($Pip)_2$] (Table S22).[59]

The X-ray orientations of the axial ligands of [Fe(TPP)-($PhCH_2CH_2NH_2)_2$] (defined by the dihedral angle ϕ, N_p−Fe−N_{ax}−C_L) are reproduced exactly in the calculated in vacuo structure (ϕ_1, ϕ_2 = 0°, 180°). In the case of [Fe(TPP)(1-$BuNH_2)_2$], the calculated axial ligand orientations (0 and 180°) differed by 15.2° from the crystallographically observed orientations. The axial ligand dihedral angles were therefore restrained at the X-ray values during geometry optimization to obtain the closest conformational fit to the crystal structure (Figure 5). A similarly restrained conformation of [Fe(TPP)($BzNH_2)_2$] was used for comparison with the X-ray structure since the calculated minimum energy orientations of the axial ligands (ϕ_1, ϕ_2 = 0, 90°; isoenergetic with 0, 180°) differed significantly from the crystallographically observed orientations (18.2 and 30.1°). No restraints were required to fit the X-ray conformation of [Fe-

(59) The calculated (gas phase) mean phenyl group orientations of the axial benzylamine and phenethylamine ligands of [Fe(TPP)($BzNH_2)_2$] and [Fe(TPP)($PhCH_2CH_2NH_2)_2$] differ from the X-ray orientations by 8.9-(21) and 12.8(9)°, respectively. These differences are consistent with crystal packing effects on the X-ray conformations.

(60) Quinn, R.; Strouse, C. E.; Valentine, J. S. *Inorg. Chem.* **1983**, *22*, 2934−3940.

(61) Little, R. G.; Dymock, K. R.; Ibers, J. A. *J. Am. Chem. Soc.* **1975**, *97*, 4532−4539.

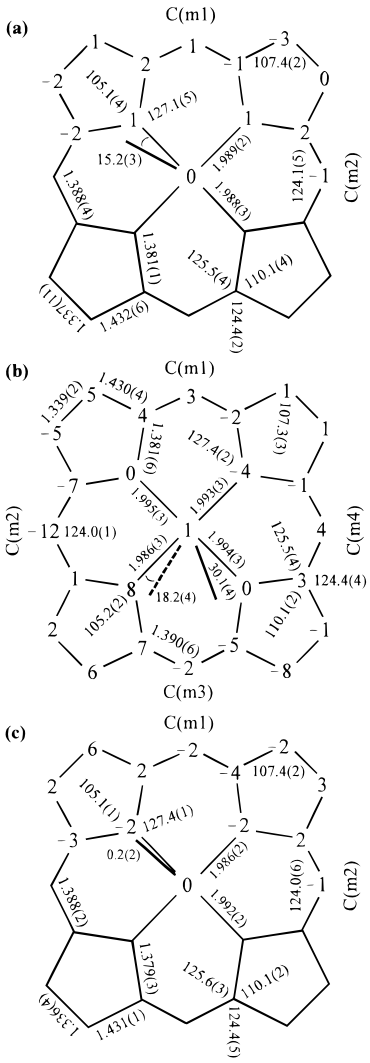

Figure 2. Formal diagrams of the porphyrin cores of (a) [Fe(TPP)(1-$BuNH_2$)$_2$], (b) [Fe(TPP)($BzNH_2$)$_2$], and (c) [Fe(TPP)($PhCH_2CH_2NH_2$)$_2$]. Averaged values (and their esd's) of the chemically unique bond distances (in Å) and angles (in deg) are shown. The perpendicular displacements (in units of 0.01 Å) of the iron and 24 porphyrin core atoms from the porphyrin mean plane are also displayed. The dihedral angle (deg) of the above-plane axial ligand ($N_p-Fe-N_{ax}-C_L$) is indicated by the solid line in each diagram. The dashed line for [Fe(TPP)($BzNH_2$)$_2$] gives the unique dihedral angle of the below-plane ligand.

(TPP)(Pip)$_2$]; the calculated minimum energy conformation (ϕ_1, ϕ_2 = 70, 110°) matches the X-ray structure and has exact inversion symmetry.

[Fe(TPP)(1-$BuNH_2$)$_2$] was used to evaluate crystal packing effects for this class of compounds. The differences between the phenyl group and axial ligand orientations of the calculated (in vacuo) and X-ray structures were significantly minimized when the geometry optimization was performed on a single molecule within its crystal lattice environment. Specifically, a markedly improved fit (rmsd = 0.026 Å) of the calculated and observed conformations was obtained if a complete set of neighboring molecules was included in the calculation. Figure 6 shows the 14 invariant structures and the geometry optimized conformation of [Fe(TPP)(1-$BuNH_2$)$_2$] calculated by this method. The "lattice" conformation was 1.6 kcal/mol higher in energy than the gas phase conformation and had similar $Fe-N_{ax}$ and $Fe-N_p$ bond distances.

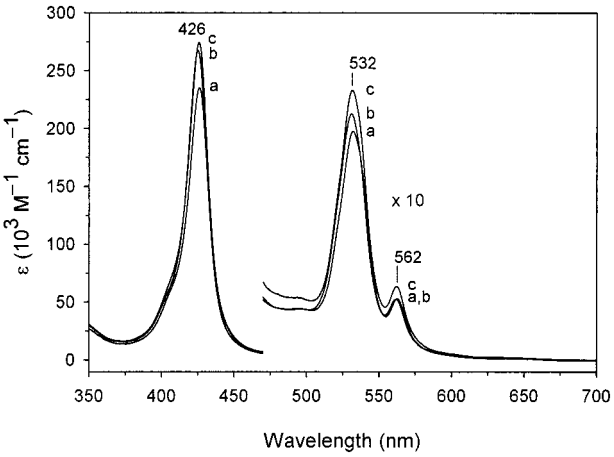

Figure 3. Electronic spectra of [Fe(TPP)(1-$BuNH_2$)$_2$] (52.6 μM, a), [Fe(TPP)($BzNH_2$)$_2$] (60.6 μM, b), and [Fe(TPP)($PhCH_2CH_2NH_2$)$_2$] (66.1 μM, c) recorded in dry CH_2Cl_2 solution at 25(1) °C under nitrogen. The free ligand (RNH_2) concentrations are 0.81 M for [Fe(TPP)(1-$BuNH_2$)$_2$], 0.29 M for [Fe(TPP)($BzNH_2$)$_2$], and 0.38 M for [Fe(TPP)($PhCH_2CH_2NH_2$)$_2$].

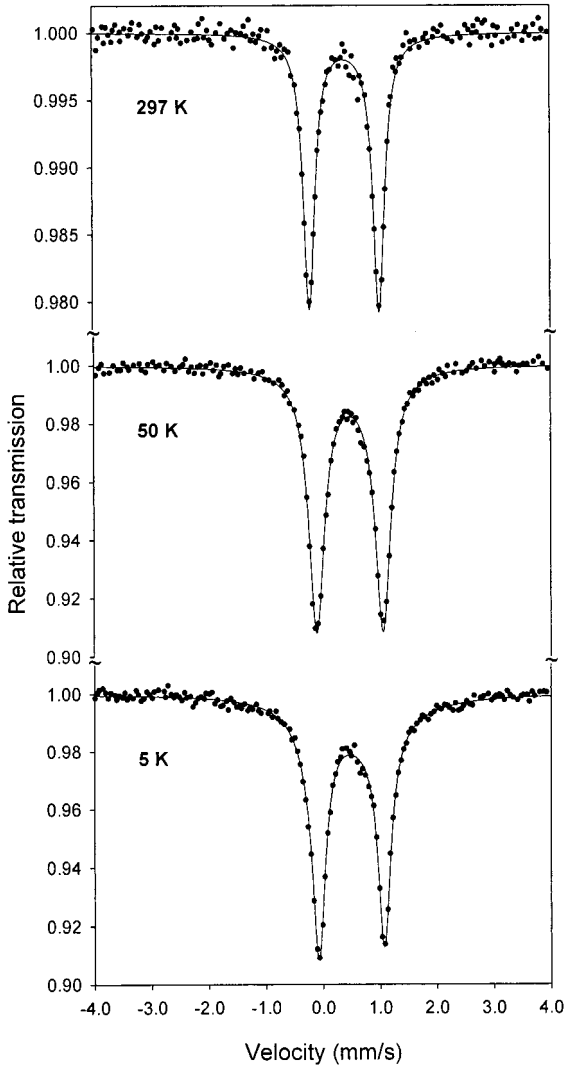

Figure 4. Zero-field Mössbauer spectra of [Fe(TPP)($BzNH_2$)$_2$] taken at 297, 50, and 5 K. The solid lines are least-squares fits of the data to the sum of two *inequivalent* quadrupole doublets.

Figure 7 compares conformational energy surfaces for [Fe(TPP)(1-$BuNH_2$)$_2$] and [Fe(TPP)(Pip)$_2$] as plots of the change

Table 2. Mössbauer Data for Bis(amine)iron(II) Porphyrin Complexes[a]

complex	T (K)	δ (mm/s)[b]	ΔE_Q (mm/s)	Γ (mm/s)[c]
[Fe(TPP)($BzNH_2$)$_2$][d]	5	0.493(1)	1.162(2)	0.16
	50	0.478(2)	1.169(2)	0.16
	80	0.480(1)	1.175(2)	0.17
	297	0.400(2)	1.204(3)	0.10
[Fe(TPP)(1-$BuNH_2$)$_2$][d]	80	0.436(2)	1.144(6)	0.13
	297	0.401(2)	1.151(3)	0.18
[Fe(TPP)($PhCH_2CH_2NH_2$)$_2$][d]	80	0.439(2)	1.147(4)	0.13
	297	0.393(1)	1.154(4)	0.15
[Fe(PPIX)(CH_3NH_2)$_2$][e]	78	0.47(1)	1.08(1)	0.17(1)
[Fe(PPIX)($EtNH_2$)$_2$][e]	78	0.47(3)	1.09(1)	0.17(1)
[Fe(PPIX)(Et_2NH)$_2$][e]	78	0.45(2)	1.07(1)	0.18(1)
[Fe(PPIX)($HO(CH_2)_2NH_2$)$_2$][e]	78	0.47(1)	1.09(1)	0.18(1)
[Fe(PPIX)($H_2N(CH_2)_2NH_2$)$_2$][e]	78	0.52(1)	1.15(1)	0.15(1)
[Fe(PPIX)(*n*-$PrNH_2$)$_2$][e]	78	0.49(1)	1.09(1)	0.22(1)
[Fe(PPIX)(*n*-$BuNH_2$)$_2$][e]	78	0.48(1)	1.03(1)	0.17(1)
[Fe(PPIX)(*sec*-$BuNH_2$)$_2$][e]	78	0.48(1)	1.09(1)	0.13(1)
[Fe(PPIX)(*n*-octylamine)$_2$][e]	78	0.48(2)	1.03(1)	0.13(2)
[Fe(PPIX)(Pip)$_2$][e]	78	0.52(1)	1.40(2)	0.16(1)
[Fe(OEP)(NH_3)$_2$][f]	4.2	0.49(1)	1.11(1)	0.31(1), 0.32(1)[g]
	115	0.51(1)	1.10(1)	0.30(1), 0.30(1)[g]
	295	0.41(1)	1.18(1)	0.23(1), 0.28(1)[g]
[Fe(TPP)(Pip)$_2$][h]	4.2	0.51(1)	1.44(1)	
	77	0.50(1)	1.44(1)	
	195	0.47(1)	1.49(1)	
	300	0.42(1)	1.52(1)	

[a] The estimated errors of the least significant digits are given in parentheses. [b] Isomer shifts are relative to metallic iron. [c] Half-width at half-maximum. [d] This work. Source line width = 0.16 mm/s. The sample line widths were fixed at the tabulated values. [e] Reference 33. [f] Reference 7. [g] Full width at half-maximum. [h] Reference 31.

in total steric energy with axial ligand orientation. (Alternative plots of $-\Delta U_T$ with ligand dihedral angle are given in Figure S1 to emphasize the energy minima.) The surface for [Fe(TPP)(1-$BuNH_2$)$_2$] exhibits numerous isoenergetic minima and maxima. Two distinct types of high-energy conformation are evident: (1) conformations in which the axial ligands are *eclipsed* and oriented over the bisector of a *cis*-N_p−Fe−N_p angle, e.g., ϕ_1, ϕ_2 = 45, 315° (ΔU_T = 0.80 kcal/mol) and (2) those with *staggered* axial ligands (relative orientations, $\Delta\phi$, of 90 or 180°) positioned over the bisector of a *cis*-N_p−Fe−N_p angle, e.g., ϕ_1, ϕ_2 = 45, 225° (ΔU_T = 0.69 kcal/mol). In both cases the α-CH_2 protons of the butylamine ligands point directly at adjacent pyrrole nitrogens (H···N_p = 2.70 Å). Two distinct classes of low-energy conformation for [Fe(TPP)(1-$BuNH_2$)$_2$] are also evident in Figure 7. The lowest energy conformers (ΔU_T = 0 kcal/mol) have *staggered* axial ligands ($\Delta\phi$ = 90 or 180°) positioned directly over a cis or trans pair of Fe−N_p bonds, e.g., ϕ_1, ϕ_2 = 0, 180°. Local minima (ΔU_T = 0.14 kcal/mol) occur when the axial ligands are exactly eclipsed ($\Delta\phi$ = 0°) and lie directly over a single Fe−N_p bond, e.g., ϕ_1, ϕ_2 = 0, 0°. These conformations stagger the α-CH_2 protons of the ligands relative to the pyrrole nitrogens (H···N_p = 2.84 Å).

The surface for [Fe(TPP)(Pip)$_2$] (Figure 7) shows two types of high-energy conformation depending on the relative orientations of the axial piperidine ligands. The changes in total steric energy with axial ligand orientation are also considerably larger (ΔU_{Tmax} ~3.8 kcal/mol) than for [Fe(TPP)(1-$BuNH_2$)$_2$], consistent with the increased steric bulk of the axial ligands. The highest energy conformations (ΔU_T ~ 3.8 kcal/mol, e.g., ϕ_1, ϕ_2 = 110, 70°) have exact inversion symmetry; the N−H bonds of the axial piperidine ligands eclipse a pair of *trans*-Fe−N_p bonds leading to N_p−Fe−N_{ax}−C_L dihedral angles of ~20° relative to the closest Fe−N_p vectors. Local energy maxima (ΔU_T ~3.0 kcal/mol) occur when the N−H bonds of the axial piperidine ligands eclipse a pair of *cis*-Fe−N_p bonds, e.g., ϕ_1, ϕ_2 = 20, 70°. For both types of maximum, the equatorial pairs of α-CH_2 protons of the ligands directly eclipse a pair of trans porphyrin nitrogens, leading to short nonbonded contacts (H···N_p = 2.43 Å) and a high steric energy.

Three distinct types of low-energy conformation are evident for [Fe(TPP)(Pip)$_2$]. In the lowest energy conformations (ΔU_T = 0 kcal/mol, e.g., ϕ_1, ϕ_2 = 70, 20°) the N−H bonds of the axial ligands are staggered (90° apart) and are positioned over the bisectors of adjacent *cis*-N_p−Fe−N_p angles. The first type of local minimum (ΔU_T ~1.6 kcal/mol, e.g., ϕ_1, ϕ_2 = 160, 20°) has exact inversion symmetry; the N−H bonds of the axial ligands are staggered (180° apart) and eclipse the bisector of a *cis*-N_p−Fe−N_p angle. In the second type of local minimum (ΔU_T ~1.8 kcal/mol, e.g., ϕ_1, ϕ_2 = 340, 20°) the N−H bonds of the axial ligands are exactly eclipsed and are positioned over the bisector of a *cis*-N_p−Fe−N_p angle. For all minimum energy conformations, the axial pairs of α-CH_2 protons of the ligands point toward a pair of cis porphyrin nitrogens, favoring longer nonbonded contacts (H···N_p 2.72 Å) than for the higher energy conformations.

Discussion

Molecular Structures. The structures of [Fe(TPP)(1-$BuNH_2$)$_2$], [Fe(TPP)($BzNH_2$)$_2$], and [Fe(TPP)($PhCH_2CH_2NH_2$)$_2$] are unique in several respects. Most importantly, they are the first X-ray structures of primary amine complexes of iron(II) porphyrins and provide unprecedented stereochemical data for the coordination of RNH_2 ligands by simple iron porphyrins. They also serve as a useful starting point from which to explore biologically relevant amine complexes of iron porphyrins. The unusual heme axial ligand combination of the plant cytochromes *f* (His−Fe−NH_2R, where NH_2R is the α-NH_2 group of Tyr-1) is of particular interest in this context since the recently reported X-ray structure of turnip cytochrome *f*[21,22] has established a definitive structural role for the alkylamine ligand. Specifically, heme incorporation and coordination of the α-NH_2 group of Tyr-1 is thought to occur after (1) translocation of the protein

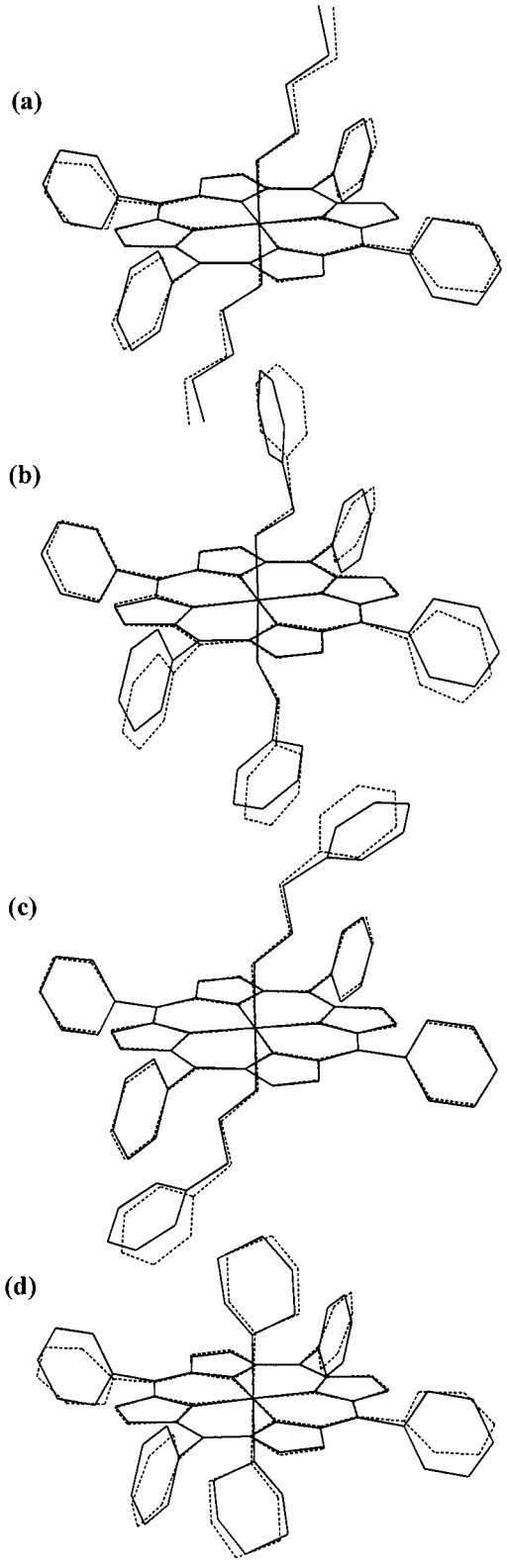

Figure 5. Comparison of MM-calculated (gas phase, solid lines) and crystallographically observed (broken lines) structures of low-spin bis(amine)iron(II) porphyrins. The X-ray structures to which the calculated structures have been fitted (and rmsd's) are (a) [Fe(TPP)(1-$BuNH_2)_2$] (0.042 Å), (b) [Fe(TPP)($BzNH_2)_2$] (0.058 Å), (c) [Fe(TPP)($PhCH_2CH_2NH_2)_2$] (0.032 Å), and (d) [Fe(TPP)($Pip)_2$] (0.073 Å). Hydrogen atoms have been omitted for clarity.

from the chloroplast stroma across the thylakoid membrane and (2) cleavage of the leader segment of the polypeptide chain. This event (heme incorporation) therefore marks the onset of

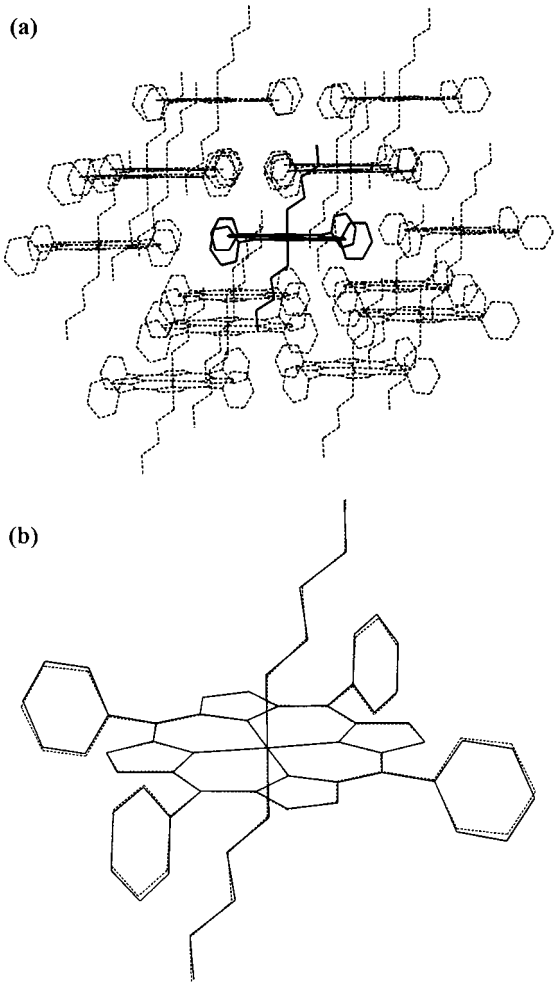

Figure 6. (a) Perspective view of the calculated structure of [Fe(TPP)(1-$BuNH_2)_2$] (solid lines) within its lattice environment. The coordinates of the Fe(II) ion and all atoms of the 14 neighboring complexes were fixed during geometry optimization of the highlighted molecule. (b) Least-squares fit of the calculated (solid lines) and X-ray structure (broken lines) of [Fe(TPP)(1-$BuNH_2)_2$] for the calculation involving 14 lattice neighbors. The rmsd (Fe, 24 porphyrin core atoms, axial nitrogens) is 0.026 Å. Hydrogen atoms have been omitted for clarity in both diagrams.

the folding process which culminates in the redox-active tertiary structure of the principal domain of the functional cytochrome.[21]

The Fe−N_{ax} bonds for [Fe(TPP)(1-$BuNH_2)_2$] (2.043 Å), [Fe(TPP)($BzNH_2)_2$] (2.039 Å), and [Fe(TPP)($PhCH_2CH_2NH_2)_2$] (2.028 Å) are identical (within four standard deviations) and average 2.037(8) Å. There are no other structurally characterized primary amine complexes in the literature for comparison. However, it is noteworthy that the mean Fe−NH_2R distance is significantly shorter than the Fe−N_{ax} distance of [Fe(TPP)($Pip)_2$] (2.127 Å), consistent with the fact that α-unsubstituted primary amines are sterically less bulky than secondary amines. The mean Fe−N_{ax} distance for the three [Fe(TPP)($RNH_2)_2$] complexes of this study is equivalent to the axial distances observed for the low-spin bis(pyridine) derivatives [Fe(TPP)($Py)_2$] (2.037 Å)[3] and [Fe(TPP)($Py)_2$]·2Py (2.039 Å).[2] However, this agreement is probably coincidental since coordinated pyridines and imidazoles with a range of electronic structures show a substantial variation in their Fe−N_{ax} distances: 1.996 Å ([Fe(TMP)(4-$CNPy)_2$]),[5] 2.004 Å ([Fe(TPP)(1-$VinIm)_2$]),[1] 2.010 Å ([Fe(TMP)(4-$MePy)_2$]),[5] and 2.026 Å ([Fe(TMP)(3-$CNPy)_2$]).[5]

Interestingly, the Fe−N_{ax} distances of [Fe(TPP)(1-$BuNH_2)_2$], [Fe(TPP)($BzNH_2)_2$], and [Fe(TPP)($PhCH_2CH_2NH_2)_2$] are all

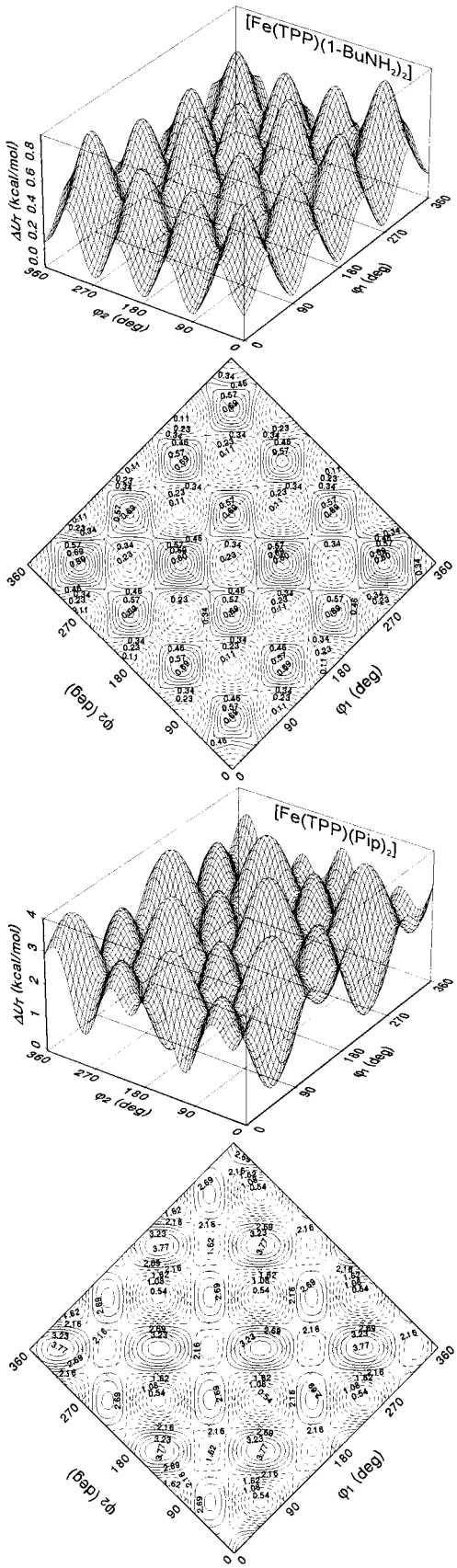

Figure 7. Plot of the change in steric energy (ΔU_T) as a function of axial amine orientation for $[Fe(TPP)(1\text{-}BuNH_2)_2]$ and $[Fe(TPP)(Pip)_2]$. A contour map of the three-dimensional surface is shown in each case; broken lines indicate regions encompassing minima on each surface. ϕ_1 and ϕ_2 correspond to the dihedral angles $N_p-Fe(II)-N_{ax}-C_L$ for the top and bottom ligands, respectively.

significantly *longer* than the $Fe-NH_2R$ distance (1.94 Å) reported for the 1.96-Å resolution X-ray structure of turnip ferrocytochrome *f*.[22] This is unexpected since the axial ligand in cytochrome *f* is an α-substituted primary amine and is therefore sterically more hindered than those of this study. Moreover, our calculations have indicated a somewhat weaker $Fe-N_{ax}$ interaction in the gas phase structure of $[Fe(TPP)(R\text{-}[+]\text{-}\alpha\text{-}MeBzNH_2)_2]$ (Figure S2), which shows equivalent $Fe-N_{ax}$ distances (2.052 Å) that are some 0.013 Å longer than those calculated for $[Fe(TPP)(BzNH_2)_2]$.

The $Fe-N_{His}$ distance (1.93 Å) of turnip cytochrome *f* is also unusually short for an iron(II) porphyrin and lies closer to that found for imidazol*ate* complexes of iron(III) porphyrins such as $[Fe(TPP)(5\text{-}MeIm)_2]^-$ (mean $Fe-N_{ax} = 1.943(21)$ Å[60]). A reasonable suggestion is that the tertiary structure of the protein coupled with the S_4-ruffled porphyrin core probably enforces a strong coordination interaction for the axial ligands in cytochrome *f*. The functional significance of this enhanced interaction is unclear. However, it is worth noting that even if the coordination distances for ferrocytochrome *f* are considered to be accurate to ±0.05 Å at 1.96-Å resolution, the $Fe-N_{ax}$ distances are still significantly shorter than those found for the $[Fe(TPP)(RNH_2)_2]$ complexes of this study and other bis(imidazole)iron(II) porphyrins.[1]

The axial ligand orientations of alkylamine complexes of iron porphyrins may be defined by the dihedral angles $N_p-Fe-N_{ax}-C_L$, where C_L is an α-CH_2 carbon. For $[Fe(TPP)(1\text{-}BuNH_2)_2]$, $[Fe(TPP)(BzNH_2)_2]$, and $[Fe(TPP)(PhCH_2CH_2NH_2)_2]$, the axial ligand dihedral angles range from ∼0 to 30.1°. The conformation of $[Fe(TPP)(PhCH_2CH_2NH_2)_2]$ is "unusual" since the axial ligands exactly eclipse a pair of *trans*-$Fe-N_p$ bonds (ϕ_1, $\phi_2 \approx$ 0, 180°). Such a conformation is rarely observed[60,61] in bis(pyridine) and bis(imidazole) complexes of iron(II/III) porphyrinates. This reflects the unfavorable steric interactions that arise when the ligand ortho protons point directly at the pyrrole nitrogens. However, in the case of α-unsubstituted primary amines, the α-CH_2 protons point away from the pyrrole nitrogens when the α-carbon and pyrrole nitrogens are eclipsed. As illustrated in Figure 8, this conformation is clearly favored on steric grounds, a finding that is supported by the MM calculations of Figures 5 and 7 (vide supra).

The fact that neither $[Fe(TPP)(1\text{-}BuNH_2)_2]$ nor $[Fe(TPP)(BzNH_2)_2]$ exhibits the same axial ligand orientations as $[Fe(TPP)(PhCH_2CH_2NH_2)_2]$ suggests an intrinsically low barrier to axial ligand rotation for α-unsubstituted primary amines. Clearly, packing interactions could easily affect the axial ligand (and porphyrin phenyl group) orientations in the solid state. The role of packing interactions is, in fact, strikingly demonstrated by the conformation of $[Fe(TPP)(1\text{-}BuNH_2)_2]$ calculated in the presence of 14 lattice neighbors (Figure 6). First, there is good agreement between the calculated and observed dihedral angles for the *meso*-phenyl groups (none deviate from the experimental values by more than 3°). This confirms the well-known[62] role of intermolecular nonbonded interactions in perturbing the phenyl group orientations of TPP derivatives. Second, in contrast to the gas phase calculation, the axial ligands no longer have a minimum energy orientation of 0° ($\phi = 7°$ in Figure 6). Although the calculated ligand orientations do not exactly match those of the X-ray structure (15.2°), the results clearly show that both the axial ligands and the *meso*-phenyl groups require some adjustments (rotations of up to ∼15°) from their in vacuo orientations before optimal packing is achieved.

(62) Scheidt, W. R.; Lee, Y. J. *Struct. Bonding* **1987**, *64*, 1−70.

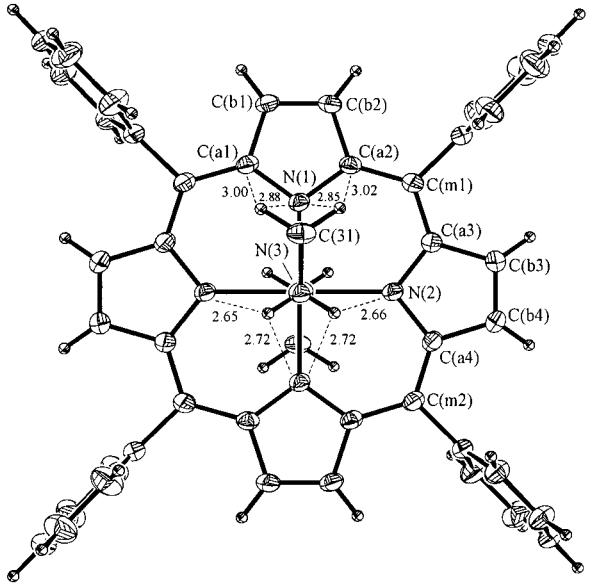

Figure 8. ORTEP diagram (ORTEX 7e)[43b] of [Fe(TPP)($PhCH_2CH_2NH_2$)$_2$] viewed down the N(3)−Fe−N(3)′ axis (approximately perpendicular to the heme plane). Only the NH_2 and α-CH_2 groups of each ligand are shown for clarity. Thermal ellipsoids are drawn at the 30% probability level. Selected nonbonded contacts are indicated by broken lines.

The nonbonded interactions which perturb the axial ligand orientations of [Fe(TPP)(1-$BuNH_2$)$_2$] have been quantified in Figure 9 which shows a stereoview of the unit cell and all atoms within a 5.0-Å radius of C(32). The relevant nonbonded contacts between phenyl group 2 of a neighboring porphyrin and the axial ligand are the following: H(32a)···C(24), 3.248 Å; H(32a)···C(25), 3.545 Å; H(31a)···C(25), 3.439 Å; H(3a)···C(25), 3.745 Å. The close proximity of this neighboring phenyl group to one side of the axial ligand clearly offsets the orientation of the ligand from its gas phase minimum (0°). A similar analysis of the packing interactions which affect the axial ligand orientations of [Fe(TPP)($BzNH_2$)$_2$] is given in Figures S3−S5.

The porphyrin cores of the three [Fe(TPP)(RNH_2)$_2$] derivatives are roughly planar. Although the individual atomic displacements are small (<0.13 Å), there is evidence for slight, *local* distortions that reflect accommodation of specific axial ligand−porphyrin core nonbonded interactions. For example, C(a6) and C(b6) of [Fe(TPP)($BzNH_2$)$_2$] (Figure 2b) are displaced below the porphyrin mean plane, while N(4), C(a7), and C(b7) are displaced above the porphyrin mean plane, consistent with the orientations of the above-plane ligand (30.1° relative to the Fe−N(3) bond) and the below-plane ligand (18.2° relative to the Fe−N(4) bond), respectively. Local distortions of this type have been noted previously for [Fe(TMP)(1,2-Me_2Im)$_2$)](ClO_4).[48]

The X-ray structures of several bis(imidazole)- and bis(pyridine)iron(II) porphyrins exhibit an average Fe−N_p distance (2.002 Å)[1−3] that is only 0.023 Å longer than the average in-plane distance for the low-spin iron(III) analogs (1.979 Å).[48,60,61,63−71] This reflects the similar iron antibonding orbital populations (<0.6 e)[8,9] for the two oxidation states, even though iron(II) has a slightly larger radius than iron(III).[72] However, it is noteworthy that, in addition to the smaller radius for iron(III), the shorter mean Fe−N_p distance for the ferric complexes

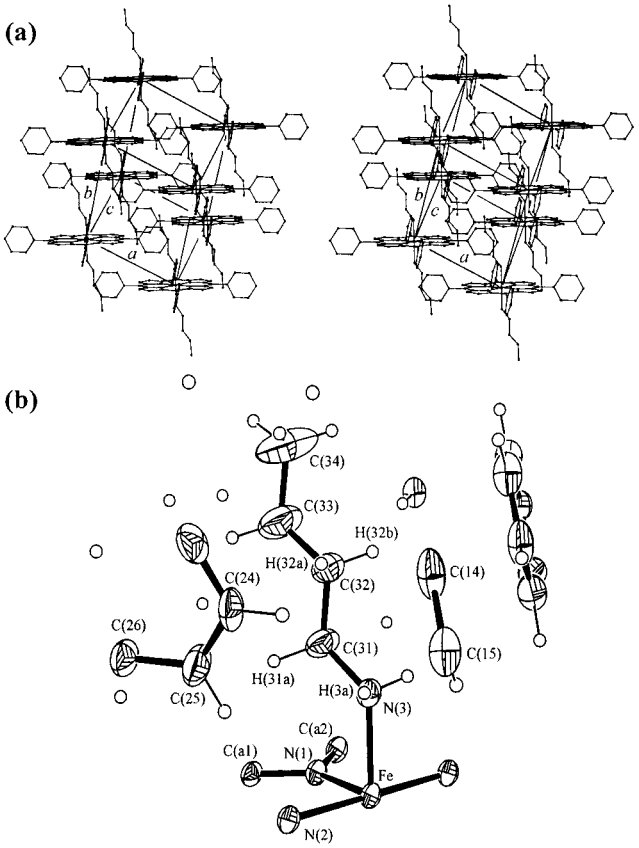

Figure 9. (a) Stereoview of the unit cell of [Fe(TPP)(1-$BuNH_2$)$_2$]. The axial butylamine ligands come into close contact with a *meso*-phenyl group of a neighboring porphyrin. (b) ORTEP diagram (30% probability surfaces for non-hydrogen atoms) showing all atoms within a 5.0-Å radius of C(32). Selected atoms have been labeled. The close nonbonded contacts which offset the ligand dihedral angle (N(1)−Fe−N(3)−C(31)) from 0° (gas-phase orientation) to 15.2° mainly involve C(24) and C(25) of the neighboring phenyl group and H(32a) of the ligand.

reflects the fact that many are S_4-ruffled.[62] In contrast, all known [Fe^{II}(porphyrin)L_2] complexes, where L = an amine, imidazole, or pyridine derivative, are planar. Since the average Fe−N_p distance for [Fe(TPP)(1-$BuNH_2$)$_2$], [Fe(TPP)($BzNH_2$)$_2$], and [Fe(TPP)($PhCH_2CH_2NH_2$)$_2$] is 1.990(2) Å, the Fe−N_p distances for bis(primary amine)iron(II) porphyrinates appear to be intrinsically shorter than those of comparable bis(imidazole) and bis(pyridine) ferrous complexes. However, this may be due to the small sample size for the three classes of compound, particularly since the mean Fe−N_p distance of [Fe(TPP)(Pip)$_2$] is 2.004(4) Å.[37]

Electronic and Mössbauer Spectroscopy. The electronic spectra of [Fe(TPP)(1-$BuNH_2$)$_2$], [Fe(TPP)($BzNH_2$)$_2$], and [Fe(TPP)($PhCH_2CH_2NH_2$)$_2$] confirm the crystallographically ob-

(63) Safo, M. K.; Gupta, G. P.; Walker, F. A.; Scheidt, W. R. *J. Am. Chem. Soc.* **1991**, *113*, 5497−5510.
(64) Safo, M. K.; Gupta, G. P.; Walker, F. A.; Watson, C. T.; Simonis, U.; Scheidt, W. R. *J. Am. Chem. Soc.* **1992**, *114*, 7066−7075.
(65) Scheidt, W. R.; Osvath, S. R.; Lee, Y. J. *J. Am. Chem. Soc.* **1987**, *109*, 1958−1963.
(66) Higgins, T.; Safo, M. K.; Scheidt, W. R. *Inorg. Chim. Acta* **1990**, *178*, 261−267.
(67) Scheidt, W. R.; Kirner, J. F.; Hoard, J. L.; Reed, C. A. *J. Am. Chem. Soc.* **1987**, *109*, 1963−1968.
(68) Inniss, D.; Soltis, S. M.; Strouse, C. E. *J. Am. Chem. Soc.* **1988**, *110*, 5644−5650.
(69) Quinn, R.; Valentine, J. S.; Byrn, M. P.; Strouse, C. E. *J. Am. Chem. Soc.* **1987**, *109*, 3301−3308.
(70) Collins, D. M.; Countryman, R.; Hoard, J. L. *J. Am. Chem. Soc.* **1972**, *94*, 2066−2072.
(71) Safo, M. K.; Walker, F. A.; Raitsimring, A. M.; Walters, W. P.; Dolata, D. P.; Debrunner, P. G.; Scheidt, W. R. *J. Am. Chem. Soc.* **1994**, *116*, 7760−7770.
(72) Scheidt, W. R.; Reed, C. A. *Chem. Rev.* **1981**, *81*, 543−555.

served low-spin Fe(II) oxidation state. Although the spectra of the three derivatives show Q and B band maxima at the same wavelengths (562, 532, and 426 nm), the molar absorptivities increase in the order [Fe(TPP)(1-BuNH$_2$)$_2$] < [Fe(TPP)(BzNH$_2$)$_2$] < [Fe(TPP)(PhCH$_2$CH$_2$NH$_2$)$_2$] at 532 and 426 nm. The enhancement of oscillator strength for the Q and B bands may reflect an exciton interaction[73] between the transition dipoles of the phenyl groups of the axial ligands and the *xy*-polarized transition dipoles of the porphyrin ring.[74] Coupling of the transition dipoles is expected to be largest in the PhCH$_2$-CH$_2$NH$_2$ complex since the phenyl substituents of the axial ligands are closer to being parallel with the heme group, at least in the solid state (Figure 1). The wavelengths of the Q and B band maxima for the three primary amine complexes compare favorably with those reported for [Fe(TPP)(1-VinIm)$_2$] and [Fe(TPP)(1-BzlIm)$_2$] (420−427 nm, B(0,0); 532−537 nm, Q$_v$; 562−566 nm Q$_o$)[1] and the bis(pyridine) derivatives [Fe(TMP)(4-CNPy)$_2$], [Fe(TMP)(3-CNPy)$_2$], and [Fe(TMP)(4-MePy)$_2$].[5]

The Mössbauer spectra of [Fe(TPP)(1-BuNH$_2$)$_2$], [Fe(TPP)(BzNH$_2$)$_2$], and [Fe(TPP)(PhCH$_2$CH$_2$NH$_2$)$_2$] show similar, weakly temperature-dependent isomer shifts (δ) and quadrupole splittings (ΔE_Q) that are consistent with a low-spin Fe(II) oxidation state[57] for the heme iron (Table 2). The δ-values of the three primary amine complexes at 80 K are, on average (0.452(2) mm/s), equivalent to those typical of bis(imidazole)- and bis(pyridine)(porphinato)iron(II) derivatives (0.44(3) mm/s)[1,7] and, more expectedly, those reported for the bis(amine) complexes of [Fe(OEP)], [Fe(TPP)], and [Fe^{II}(PPIX)].[7,32,33] The total metal s-electron density in Fe(II) porphyrins therefore appears to be relatively insensitive to the type of axial N-donor ligand and porphyrin ligand coordinated to the metal.

The quadrupole splittings of [Fe(TPP)(1-BuNH$_2$)$_2$], [Fe(TPP)(BzNH$_2$)$_2$], and [Fe(TPP)(PhCH$_2$CH$_2$NH$_2$)$_2$] average 1.16(2) mm/s at 80 K and are within the range of ΔE_Q values observed for [Fe(TPP)(NH$_3$)$_2$] (1.10−1.18 mm/s)[7] and the ferrous protoporphyrin IX complexes (1.07−1.15 mm/s)[33] in Table 2. However, the ΔE_Q values of [Fe(TPP)(Pip)$_2$] are significantly larger (1.44−1.52 mm/s) than those of the RNH$_2$ complexes, consistent with a larger difference between the Fe−N$_p$ (2.004 Å) and Fe−N$_{ax}$ (2.127 Å) bonds[37] and, consequently, a larger EFG at the nucleus. The slightly larger ΔE_Q values for [Fe(TPP)(BzNH$_2$)$_2$] relative to [Fe(TPP)(1-BuNH$_2$)$_2$] and [Fe(TPP)(PhCH$_2$CH$_2$NH$_2$)$_2$] (Table 2) reflect the noncentrosymmetric coordination geometry of the benzylamine derivative.[75] Interestingly, the ΔE_Q values of several bis(pyridine)iron(II) porphyrinates (1.18(5) mm/s)[7] are comparable to those of the [Fe(TPP)(RNH$_2$)$_2$] complexes. This is consistent with the similar axial and equatorial coordination distances for these two classes of (porphinato)iron(II) complex (vide supra). The ΔE_Q values of the RNH$_2$ complexes (Table 2) are, however, larger than those reported for several centrosymmetric bis(imidazole)iron(II) porphyrins (1.02(3) mm/s).[1] A likely explanation is that the latter complexes show a smaller Fe−N$_{ax}$/Fe−N$_p$ structural anisotropy.

Molecular Mechanics Calculations. The objectives of this study were to determine the optimum (gas phase) axial ligand orientations and conformations for low-spin iron(II) complexes of the type [Fe(TPP)L$_2$], where L = a primary or secondary amine, and to use this information to delineate the factors which control the axial ligand orientations of [Fe(TPP)(1-BuNH$_2$)$_2$], [Fe(TPP)(BzNH$_2$)$_2$], [Fe(TPP)(PhCH$_2$CH$_2$NH$_2$)$_2$], and [Fe(TPP)(Pip)$_2$].[37]

The conformational energy surface for [Fe(TPP)(1-BuNH$_2$)$_2$] shown in Figure 7 is representative of the three [Fe(TPP)(RNH$_2$)$_2$] complexes of this study. The axial ligands of the lowest energy conformations (ΔU_T = 0 kcal/mol) *exactly* eclipse a pair of cis or trans Fe−N$_p$ bonds, leading to staggered arrangements with $\Delta\phi$ = 90 or 180°, respectively (Figure S6). From Figure 8, such a conformation clearly leads to optimal N−H···N$_p$ and α-C−H···N$_p$ nonbonded distances. Local minima (ΔU_T = 0.14 kcal/mol) are observed when the axial ligands eclipse the *same* Fe−N$_p$ bond in the porphyrin core. Since the calculated in vacuo barriers to conformational interconversion (0.34 and 0.46 kcal/mol)[76] are low for [Fe(TPP)(1-BuNH$_2$)$_2$], considerable rotational freedom should exist both in the gas phase and in solution (for which slightly higher barriers are expected[77]). However, close nonbonded contacts in the solid state (Figure 9) probably restrict rotation of the axial ligands in the lattice. This is reflected by the absence of disorder for the alkylamine ligands of this study, a situation which is not mirrored in the analogous [Co(TPP)(RNH$_2$)$_2$]SbF$_6$ compounds which crystallize in different space groups.[78]

Comparison of the calculated minima in Figure 7 and the X-ray data suggests that crystal packing effects, which perturb the orientations of the axial ligands and *meso*-phenyl groups, are manifest to a lesser or greater degree depending on the axial ligands. Thus, the X-ray structure of [Fe(TPP)(PhCH$_2$CH$_2$NH$_2$)$_2$] (ϕ_1, $\phi_2 \approx 0$, 180°) is largely unperturbed and is located virtually at the strain energy minimum on the potential surface.[79] The axial ligands of the X-ray conformation of [Fe(TPP)(1-BuNH$_2$)$_2$] (ϕ_1, ϕ_2 = 15.2, 164.8°) are moderately perturbed (Figure 9). The structure lies close to the calculated minimum (ϕ_1, ϕ_2 0, 180°) and is therefore only slightly higher in energy (∼0.13 kcal/mol). However, when packing-induced rotations of the *meso*-phenyl groups are also taken into account (Figure 6), the calculated conformation more closely matches the X-ray structure and has an even higher relative energy (∼1.6 kcal/mol). The noncentrosymmetric X-ray structure of [Fe(TPP)(BzNH$_2$)$_2$] lies furthest from a calculated energy minimum (ϕ_1, ϕ_2 = 30.1, 288.2° in Figure 7), consistent with significant packing effects on the orientations of the axial ligands. Inspection of the unit cell for [Fe(TPP)(BzNH$_2$)$_2$] (Figure S3) and the lattice environment within a 5.1-Å radius of C(52) and C(63) of the axial ligands (Figures S4 and S5) indicates that the X-ray conformation is stabilized by a $\pi-\pi$ interaction between a ligand phenyl group (C(52)−C(57)) and a phenyl ring of a neighboring porphyrin. Moreover, short nonbonded contacts with C(63) of the second phenyl group clearly cant the C(61)−C(62) bond relative to the heme normal. These intermolecular interactions

(73) Munro, O. Q.; Marques, H. M. *Inorg. Chem.* **1996**, *35*, 3768−3779.
(74) Eaton, W. A.; Hofrichter, J. In *Methods in Enzymology*, Antonini, E., Rossi-Barnardi, L., Chiancone, E., Eds.; Academic: New York, 1981; Vol. 76, pp 175−261.
(75) The following structurally characterized low-spin iron(II) porphyrins are all centrosymmetric: [Fe(TPP)(1-VinIm)$_2$],[1] [Fe(TPP)(1-BzlIm)$_2$],[1] [Fe(TPP)(Py)$_2$],[3] [Fe(TPP)(Py)$_2$]·2Py,[2] [Fe(TMP)(4-CNPy)$_2$],[5] [Fe(TMP)(3-CNPy)$_2$],[5] and [Fe(TMP)(4-MePy)$_2$].[5] [Fe(TPP)(BzNH$_2$)$_2$] is the first example of a noncentrosymmetric bis(N-donor)(porphinato)iron(II) complex.
(76) There are two types of rotational barrier for the primary amine ligands of [Fe(TPP)(RNH$_2$)$_2$] derivatives. These are exemplified by the saddle points with coordinates ϕ_1, ϕ_2 = 90, 45° (0.34 kcal/mol) and ϕ_1, ϕ_2 = 180, 135° (0.46 kcal/mol).
(77) Whitenell, R. M.; Wilson, K. R. In *Reviews in Computational Chemistry*; Lipkowitz, K. B., Boyd, D. B., Eds.; VCH: New York, 1993; Vol. IV, pp 67−148.
(78) Munro, O. Q.; Shabalala, S. C.; Brown, N. J. Unpublished work.
(79) The crystal structure is not the true global minimum since the C$_a$−C$_m$−C$_p$−C$_p$ dihedral angles (Table 1) deviate from the calculated minimum energy value of 90° by up to 4.8°. This tilting of the *meso*-aryl groups in the crystal structure reflects modest intermolecular nonbonded (packing) interactions.[62]

collectively favor the noncentrosymmetric conformation even though it has a higher energy (~0.5 kcal/mol) than the in vacuo minimum.

The surface for [Fe(TPP)(Pip)$_2$] (Figure 7) shows more distinct local minima and maxima than the surface for [Fe(TPP)(1-BuNH$_2$)$_2$]. This is mainly due to the increase in axial ligand steric bulk in the bis(piperidine) derivative which leads to larger rotational barriers for the axial ligands (e.g., ~2.2 kcal/mol at ϕ_1, ϕ_2 = 70, 70°). The saddle point conformations of [Fe(TPP)(Pip)$_2$] are characterized by a partly staggered axial ligand arrangement in which the N−H group of one ligand eclipses an Fe−N$_p$ bond while the N−H group of the trans ligand eclipses the bisector of a *cis*-N$_p$−Fe−N$_p$ angle in the porphyrin core. The latter ligand orientation places the axial pair of α-CH$_2$ protons directly over adjacent pyrrole nitrogens, leading to much of the increase in steric energy relative to the minimum (vide supra).

The lowest energy conformations of [Fe(TPP)(Pip)$_2$] (e.g., ϕ_1, ϕ_2 = 70, 20°) have S_4-ruffled porphyrin cores (Figure S6) with mean Fe−N$_{ax}$ and Fe−N$_p$ distances of 2.110(0) and 1.991(3) Å, respectively. In contrast, the calculated conformation that best models the X-ray structure of [Fe(TPP)(Pip)$_2$][37] (ϕ_1, ϕ_2 = 70, 110°) is a local minimum ($\Delta U_T \approx 1.6$ kcal/mol) with exact inversion symmetry and a planar porphyrin core. The calculated coordination group distances (Fe−N$_{ax}$ = 2.128 Å, Fe−N$_p$ = 2.000 Å) are also considerably longer than those of the S_4-ruffled conformations. Thus, as for planar and S_4-ruffled bis(imidazole) complexes of iron(III) porphyrins,[48,62] a measurable contraction of the Fe−N$_p$ bonds is predicted for S_4-ruffled iron(II) porphyrins.[80] As noted earlier, the calculated energy minima for [Fe(TPP)(Pip)$_2$] in Figure 7 reflect the fact that stable conformations arise when the equatorial pairs of α-CH$_2$ protons eclipse cis porphyrin nitrogens since this leads to the least repulsive set of nonbonded contacts. This conclusion is consistent with the MM data recently reported for [Ni(TPP)(Pip)$_2$] by Shelnutt and coworkers.[81] Thus, as for the primary amine derivatives (Figure 8), optimization of the α-C−H···N$_p$ and N−H···N$_p$ nonbonded interactions dictates the preferred axial ligand orientations.[82]

(80) This prediction awaits experimental confirmation since there are currently no X-ray structures of S_4-ruffled low-spin (porphinato)iron(II) derivatives with N-donor axial ligands.

(81) Jia, S. L.; Jentzen, W.; Shang, M.; Song, X. Z.; Ma, J. G.; Scheidt, W. R.; Shelnutt, J. A. *Inorg. Chem.* **1998**, *37*, 4402−4412.

(82) The crystallographically required inversion symmetry of [Fe(TPP)(Pip)$_2$][37] leads to selection of a local minimum energy structure rather than the global minimum. A more favorable lattice enthalpy presumably outweighs the increase in strain energy (~1.6 kcal/mol) of the more symmetrical conformation.

Conclusion

The structures of three novel bis(primary amine)(porphinato)iron(II) complexes, [Fe(TPP)(1-BuNH$_2$)$_2$], [Fe(TPP)(BzNH$_2$)$_2$], and [Fe(TPP)(PhCH$_2$CH$_2$NH$_2$)$_2$], have been determined. Of particular interest is the mean Fe−N$_{ax}$ distance (2.037 Å) which is considerably longer than the Fe(II)−amine distance of turnip cytochrome *f* (1.94 Å) but shorter than that of [Fe(TPP)(Pip)$_2$] (2.127 Å). The Mössbauer spectra of the three [Fe(TPP)(RNH$_2$)$_2$] derivatives confirm the low-spin Fe(II) oxidation state and show comparable quadrupole splittings and isomer shifts to several bis(pyridine)- and bis(alkylamine)iron(II) porphyrins.

MM calculations (in vacuo) indicate that the preferred orientations of the axial ligands of [Fe(TPP)(RNH$_2$)$_2$] derivatives position the ligand α-carbons directly over the pyrrole nitrogens of the porphyrin core, thereby minimizing the axial ligand α-C−H···N$_p$ nonbonded interactions. Although the lowest energy conformations of [Fe(TPP)(Pip)$_2$] are S_4-ruffled and have the axial ligand α-carbons oriented at 20° relative to the nearest Fe−N$_p$ bonds, this conformation also minimizes α-C−H···N$_p$ nonbonded contacts. MM calculations on a single [Fe(TPP)(1-BuNH$_2$)$_2$] complex within its crystal lattice environment have been used to show that intermolecular nonbonded interactions significantly influence the observed orientations of the axial ligands and the *meso*-phenyl groups in these TPP derivatives.

Acknowledgment. We thank (1) the URF, University of Natal, for financial support, (2) Niyum S. Ramesar for her assistance with X-ray data collections, and (3) Professors John S. Field and Raymond J. Haines for their helpful suggestions (O.Q.M.). G.H. thanks the University of the Witwatersrand and the National Research Foundation, Pretoria, for financial support.

Supporting Information Available: Complete crystallographic details, atomic coordinates, anisotropic thermal parameters, fixed hydrogen atom coordinates, bond lengths, bond angles, and dihedral angles for [Fe(TPP)(1-BuNH$_2$)$_2$], [Fe(TPP)(BzNH$_2$)$_2$], and [Fe(TPP)(PhCH$_2$CH$_2$NH$_2$)$_2$] (Tables S1−S21), X-ray crystallographic files in CIF format, comparisons of crystallographic and MM-calculated geometric parameters for [Fe(TPP)(1-BuNH$_2$)$_2$], [Fe(TPP)(BzNH$_2$)$_2$], [Fe(TPP)(PhCH$_2$CH$_2$NH$_2$)$_2$], and [Fe(TPP)(Pip)$_2$] (Tables S22−S28), and plots of $-\Delta U_T$ with axial ligand orientation for [Fe(TPP)(1-BuNH$_2$)$_2$] and [Fe(TPP)(Pip)$_2$], an MM-calculated structure of [Fe(TPP)(*R*-[+]-α-MeBzNH$_2$)$_2$], a unit cell diagram for [Fe(TPP)(BzNH$_2$)$_2$], ORTEP diagrams of all atoms within a 5.1-Å radius of C(63) and C(52) of [Fe(TPP)(BzNH$_2$)$_2$], and stereoscopic views of selected calculated minima for [Fe(TPP)(1-BuNH$_2$)$_2$] and [Fe(TPP)(Pip)$_2$] taken from the surfaces in Figure 7 (Figures S1−S6). This material is available free of charge via the Internet at http://pubs.acs.org.

IC990178Q